Title:

Ether Lipid Biosynthesis Promotes Lifespan Extension and Enables Diverse Prolongevity Paradigms in *Caenorhabditis elegans*

Lucydalila Cedillo[1,2,3], Sainan Li[1,2], Fasih M. Ahsan[1,2,3], Nicole L. Stuhr[7], Yifei Zhou[1,2], Yuyao Zhang[1,2], Adebanjo Adedoja[1,2,3], Luke M. Murphy[1,2,3], Armen Yerevanian[1,2], Sinclair Emans[1,2], Khoi Dao[4], Zhaozhi Li[5], Nicholas D. Peterson[6], Jeramie Watrous[4], Mohit Jain[4], Sudeshna Das[5], Read Pukkila-Worley[6], Sean P. Curran[7] and Alexander A. Soukas[1,2,*]

[1]Center for Genomic Medicine and Diabetes Unit, Endocrine Division, Department of Medicine, Massachusetts General Hospital and Harvard Medical School, Boston MA 02114

[2]Broad Institute of Harvard and MIT, Cambridge, MA 02142

[3]Program in Biological and Biomedical Sciences, Division of Medical Sciences, Harvard Medical School, Boston, MA 02114

[4]Department of Medicine and Pharmacology, University of California San Diego, San Diego, CA 92093

[5]Biomedical Informatics Core, Massachusetts General Hospital and Harvard Medical School, Cambridge, MA 02139

[6]Program in Innate Immunity, Division of Infectious Diseases and Immunology, University of Massachusetts Medical School, Worcester, MA, 01655

[7]Leonard Davis School of Gerontology, University of Southern California, Los Angeles, CA, 90089

For Correspondence: Alexander A. Soukas

Email: asoukas@mgh.harvard.edu

Author Contributions: Conceptualization, LC, AAS; Methodology, LC, SL, YZho, YZha, AA, JW, MJ, NS, SPC, AAS; Validation: LC, SL, LM, FMA, AAS; Formal Analysis: LC, FMA, JW, MJ, ZL, SD, NDP, RPW, AAS; Investigation: LC, SL, FMA, NS, YZho, YZha, AA, LM, AY, SE, KD, JW, MJ, NDP, RPW, SPC, AAS; Writing – Original Draft: LC, AAS; Writing – Review & Editing: LC, SL, FMA, NS, YZho, YZha, AA, LM, AY, SE, KD, JW, MJ, ZL, SD, NDP, RPW, SPC, AAS; Visualization: LC, FMA, ZL, NS, SD, SPC, AAS; Supervision: AAS; Funding Acquisition: AAS.

Competing Interest Statement: The authors declare that no competing interests exist.

Keywords: metformin; aging; ether lipids; *C. elegans*; metabolism

This PDF file includes:

Main Text

Figures 1 to 7

Abstract

Biguanides, including the world's most commonly prescribed drug for type 2 diabetes, metformin, not only lower blood sugar, but also promote longevity in preclinical models. Epidemiologic studies in humans parallel these findings, indicating favorable effects of metformin on longevity and on reducing the incidence and morbidity associated with aging-related diseases. In spite of this promise, the full spectrum of molecular effectors responsible for these health benefits remains elusive. Through unbiased screening in *C. elegans*, we uncovered a role for genes necessary for ether lipid biosynthesis in the favorable effects of biguanides. We demonstrate that biguanides prompt lifespan extension by stimulating ether lipid biogenesis. Loss of the ether lipid biosynthetic machinery also mitigates lifespan extension attributable to dietary restriction, target of rapamycin (TOR) inhibition, and mitochondrial electron transport chain inhibition. A possible mechanistic explanation for this finding is that ether lipids are required for activation of longevity-promoting, metabolic stress defenses downstream of the conserved transcription factor Nrf2/*skn-1*. In alignment with these findings, overexpression of a single, key, ether lipid biosynthetic enzyme, *fard-1*/FAR1, is sufficient to promote lifespan extension. These findings illuminate the ether lipid biosynthetic machinery as a novel therapeutic target to promote healthy aging.

Introduction

Metformin is first line therapy for type 2 diabetes and the most frequently prescribed oral hypoglycemic medication worldwide (Inzucchi et al., 2012). Human epidemiologic studies note an association between metformin use and decreased incidence of cancer (Evans et al., 2005; Yuan et al., 2013). In addition, metformin extends lifespan in invertebrate and vertebrate models (Cabreiro et al., 2013; Martin-Montalvo et al., 2013; Onken and Driscoll, 2010), and therefore may reduce aging-related diseases in humans (Barzilai et al., 2016). Nonetheless, our understanding of the molecular pathways governing the health-promoting effects of metformin is only just beginning to emerge. Our previous work identified a conserved signaling axis connecting mitochondria, the nuclear pore complex, and mTORC1 inhibition that is required for metformin-mediated extension of lifespan in *C. elegans* and inhibition of growth in worms and human cancer cells (Wu et al., 2016). The energy sensor AMP-activated protein kinase (AMPK) is not necessary for metformin-induced growth inhibition in *C. elegans* but is required for the drug's prolongevity effects (Cabreiro et al., 2013; Chen et al., 2017; Onken and Driscoll, 2010). Consistently, mechanistic studies indicate that the longevity-promoting transcription factor Nrf2/*skn-1* is required for biguanide-mediated lifespan extension (Cabreiro et al., 2013; Onken and Driscoll, 2010). The relationship of these metformin longevity response elements to each other and their hierarchy in the biguanide response other remains unknown. Thus, the mechanisms by which

86 metformin exacts its beneficial effects on health are likely to be branching and
87 complex.
88 The importance of ether lipids, a major structural component of cell
89 membranes, to aging and longevity is not fully established. Ether lipids are involved
90 in the maintenance of general membrane fluidity and in the formation of lipid rafts
91 within microdomains, which are important for promotion of membrane fusion and
92 cellular signaling (Glaser and Gross, 1994; Komljenovic et al., 2009; Marrink and
93 Mark, 2004). Ether lipids have broad roles in the regulation of cell differentiation
94 (Davies et al., 2001; Facciotti et al., 2012; Rodemer et al., 2003; Teigler et al.,
95 2009), cellular signaling (Albert et al., 2003; Thukkani et al., 2002), and reduction
96 of oxidative stress through their action as antioxidants (Maeba et al., 2002; Morand
97 et al., 1988; Reiss et al., 1997; Zoeller et al., 1988). Humans deficient in ether lipid
98 biogenesis suffer from rhizomelic chondrodysplasia punctata (RCDP), a rare
99 genetic disorder, which results in skeletal and facial abnormalities, psychomotor
100 retardation, and is uniformly fatal typically before patients reach their teenage
101 years (White et al., 2003). Thus, evidence linking alterations in ether lipid levels to
102 aging and longevity in humans is strictly correlative (Gonzalez-Covarrubias et al.,
103 2013; Pradas et al., 2019).
104 Ether lipids, which are structurally distinct from canonical phospholipids,
105 have a unique biosynthetic pathway through which a fatty alcohol is conjugated to
106 the glycerol backbone at the *sn-1* position via an ether linkage. Ether lipid
107 precursors are first synthesized by enzymes associated with the membranes of
108 peroxisomes (Ghosh and Hajra, 1986; Hardeman and Van den Bosch, 1989; Singh
109 et al., 1993). The main enzymes involved in ether lipid biosynthesis within the
110 peroxisomal matrix are glyceronephosphate O-acyltransferase (GNPAT) and
111 alkylglycerone phosphate synthase (AGPS). Fatty acyl-CoA reductase 1 (FAR1)
112 supplies most of the fatty alcohols used to generate the ether linkage in the
113 precursor, 1-O-alkyl-glycerol-3-phosphate. This precursor is then trafficked to the
114 endoplasmic reticulum (ER) for acyl chain remodeling to produce various ether
115 lipid products (Hua et al., 2017). In *C. elegans,* loss-of-function mutations of any
116 of the three main enzymes involved in human ether lipid biosynthesis, *acl-*
117 *7*/GNPAT, *ads-1*/AGPS, and *fard-1*/FAR1, results in an inability to produce ether
118 linked lipids, as in humans, and has been reported to shorten lifespan (Drechsler
119 et al., 2016; Shi et al., 2016). Worms and human cells deficient in ether lipids
120 exhibit compensatory changes in phospholipid species, including increases in
121 phosphatidylethanolamines and phosphatidylcholines containing saturated fatty
122 acids (Benjamin et al., 2013; Rodemer et al., 2003). However, in contrast to
123 humans, ether lipid deficient nematodes develop to adulthood at a normal rate,
124 providing an opportunity to determine the biological roles of ether lipids in aging
125 and longevity without pleiotropies associated with developmental rate.
126 Here, we show that the ether lipid biosynthetic machinery is necessary for
127 lifespan extension stimulated by metformin or the related biguanide phenformin in
128 *C. elegans*. Metabolomic analysis indicates that phenformin treatment drives
129 increases in multiple phosphatidylethanolamine-containing ether lipids.

Interestingly, requirement for the ether lipid biosynthetic genes extends to multiple genetic longevity paradigms including defective mitochondrial electron transport function (*isp-1*), defective pharyngeal pumping/ caloric restriction (*eat-2*), and compromises in mTOR complex 1 activation (*raga-1*). We show that overexpressing *fard-1*, the enzyme that supplies all the fatty alcohols for ether lipid biogenesis in *C. elegans*, extends lifespan, supportive of the idea that alterations in the ether lipid landscape alone is sufficient to promote healthy aging. Mechanistically, ether lipids promote longevity downstream of biguanide action through activation of metabolic stress defenses through the transcription factor *skn-1*/*Nrf2*. These data suggest that a heretofore unappreciated role for ether lipids is to promote organismal-level, longevity-promoting stress defenses.

Results

Genes responsible for ether lipid biosynthesis are necessary for biguanide-induced lifespan extension

A screen of ~1000 metabolic genes for RNA interference (RNAi) knockdowns that interfere with the growth-inhibitory properties of metformin in *C. elegans* (Wu et al., 2016), yielded *fard-1* and *acl-7*, which are required for ether lipid biosynthesis. Ether lipids are distinguished from canonical phospholipids as the latter contain exclusively fatty acids conjugated to glycerol, whereas ether lipids contain a fatty alcohol conjugated to the glycerol backbone at the *sn-1* position via an ether linkage (Figure 1A). Confirming our screen results, quantitative analysis following RNAi knockdown of *fard-1* and *acl-7* results in significant resistance to biguanide-induced growth inhibition (Figure 1—figure supplement 1A). Our lab has previously demonstrated that biguanide effects on growth in *C. elegans* share significant overlap mechanistically with the machinery by which metformin extends lifespan in the worm (Wu et al., 2016). Indeed, loss-of-function mutations in any of three genes encoding enzymes required for ether lipid biosynthesis, *fard-1*, *acl-7* or *ads-1*, completely abrogates lifespan extension induced by both metformin and the related biguanide phenformin (Figure 1B—G, and throughout manuscript see Supplementary file 1 for all tabular survival statistics and biological replicates). Confirming that these mutations confer resistance to metformin by compromising ether lipid synthetic capacity, RNAi knockdowns of *fard-1* and *acl-7* also partially impair lifespan extension promoted by phenformin (Figure 1—figure supplement 1B—C). Studies from this point forward are presented predominantly with phenformin because phenformin is more readily absorbed without need for a specific transporter, unlike metformin (Segal et al., 2011; Sogame et al., 2009; Wu et al., 2016), and our experience indicates more consistent lifespan extension with phenformin in *C. elegans*.

170 **Figure 1**

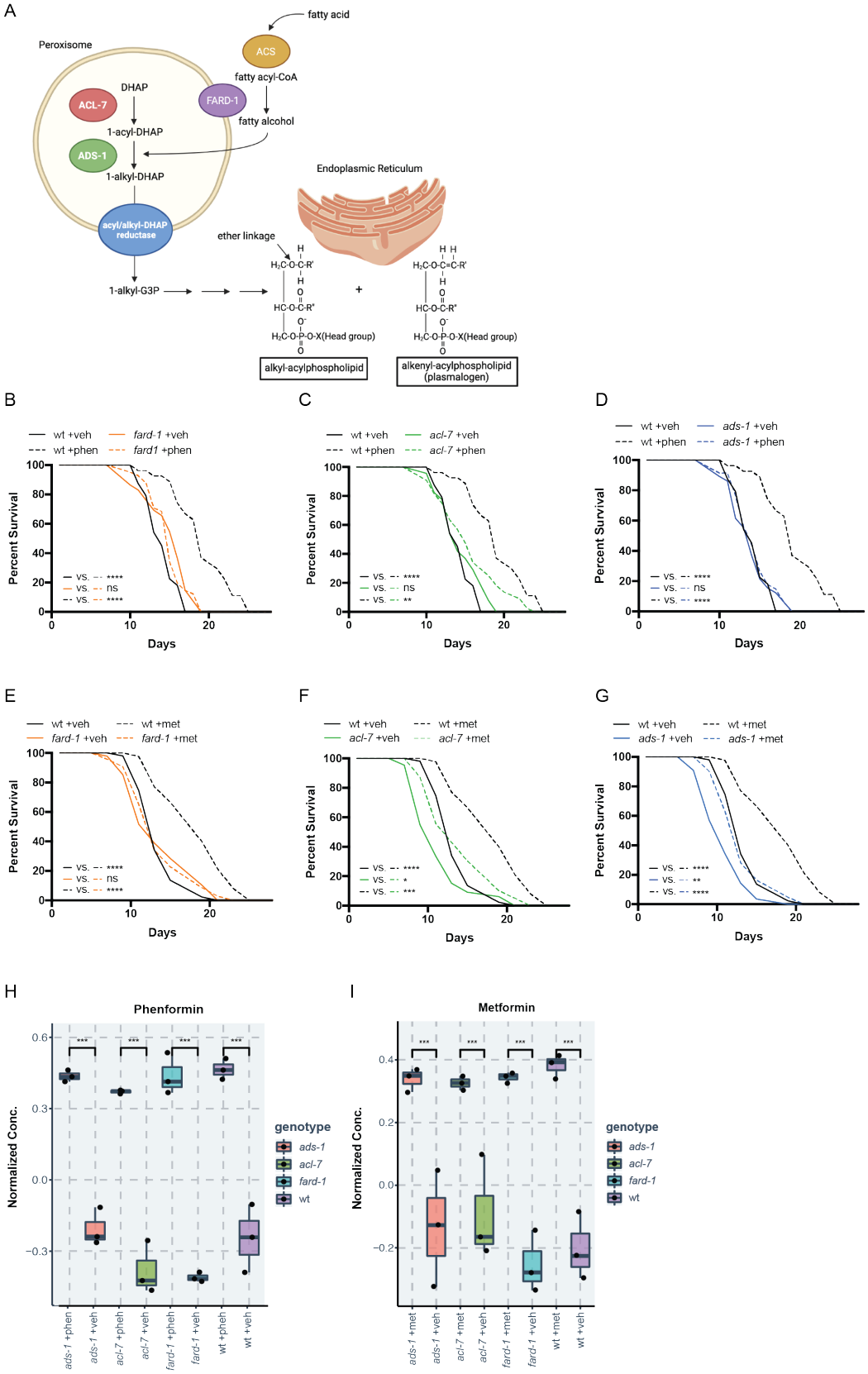
A
fatty acid
Peroxisome
ACS
fatty acyl-CoA
DHAP
ACL-7
FARD-1
fatty alcohol
1-acyl-DHAP
ADS-1
1-alkyl-DHAP
Endoplasmic Reticulum
acyl/alkyl-DHAP reductase
ether linkage
1-alkyl-G3P
alkyl-acylphospholipid
alkenyl-acylphospholipid (plasmalogen)
B
C
D
E
F
G
Percent Survival
Days
wt +veh
wt +phen
fard-1 +veh
fard1 +phen
acl-7 +veh
acl-7 +phen
ads-1 +veh
ads-1 +phen
wt +met
fard-1 +met
acl-7 +met
ads-1 +met
H
Phenformin
I
Metformin
Normalized Conc.
genotype
ads-1
acl-7
fard-1
wt

171 **Figure 1. Genes responsible for ether lipid biosynthesis are necessary for**
172 **biguanide-induced lifespan extension.** (A) *C. elegans* ether lipid synthesis is catalyzed
173 by three enzymes: fatty acyl reductase FARD-1, acyltransferase ACL-7 and alkylglycerone
174 phosphate synthase ADS-1 (adapted from (Dean and Lodhi, 2018; Shi et al., 2016)). The
175 latter two are localized to the peroxisomal lumen. (B-D) Missense, loss of function
176 mutations in *fard-1* (B), acl-7 (C), and *ads-1* (D) in *C. elegans* suppress phenformin-
177 induced lifespan extension. (E-G) A deficiency of ether lipid synthesis in *fard-1* (E), *acl-7*
178 (F), and *ads-1* (G) worm mutants blunts metformin-induced lifespan extension. Results
179 are representative of 3 biological replicates. *, $P < 0.05$; **, $P < 0.01$; ***, $P < 0.001$; ****,
180 $P < 0.0001$ by log-rank analysis. See also Figure 1-figure supplement 1 and refer to
181 Supplementary file 1 for tabular survival data and biological replicates. (H-I) Normalized
182 concentrations of phenformin (H) and metformin (I) in vehicle, 4.5mM phenformin, or 50
183 mM metformin treated wild type (wt) *C. elegans* versus *fard-1*, *acl-7*, and *ads-1* mutants.
184 n = 3 biological replicates; ***, $P < 0.004$ by two-tailed students *t*-test with Bonferroni
185 correction for multiple hypothesis testing. Box represents $75^{th}/25^{th}$ percentiles, while
186 whisker represents higher/lower hinge +/- [1.5 * interquartile range (IQR)].

187 Because ether lipids are a major structural component of cell membranes,
188 one possibility is that deficiencies in ether lipid synthesis compromises drug
189 action by reducing biguanide bioavailability in the worm. To test this, we
190 compared the relative levels of biguanides present in vehicle- and biguanide-
191 treated wild type to the three ether lipid synthesis mutants by liquid
192 chromatography—tandem mass spectrometry (LC-MS/MS). A comparison of
193 normalized concentrations of phenformin across all four strains shows that
194 phenformin abundance is quantitatively similar across wild type and the three,
195 ether lipid mutant strains (Figure 1H and Figure 1—figure supplement 1D).
196 Similar results were obtained when comparing levels of metformin wild type and
197 ether lipid mutant animals (Figure 1I and Figure 1—figure supplement 1E). Thus,
198 a deficiency in ether lipid synthesis does not significantly impact levels of
199 biguanides in *C. elegans.*
200
201 **Phenformin induces changes in ether lipid levels**
202 We reasoned that if biguanides require ether lipid biosynthesis to promote lifespan
203 extension that phenformin may promote synthesis of one or more ether lipids. To
204 investigate the impact of biguanides on ether lipids at a high level, we first utilized
205 gas chromatography-mass spectrometry (GC-MS) analysis. We first recapitulated
206 the observation that *fard-1* mutants show absence of 18-carbon containing fatty
207 acid derivatives (dimethylacetals, or DMAs, which indicate alkenyl ether lipid or
208 plasmalogen levels) and an accumulation of stearate (18:0) relative to wild type
209 controls by GC-MS (Figure 2A—B) (Shi et al., 2016). We then asked if phenformin
210 impacts the levels of 18-carbon alkenyl ether lipids in wild type animals and if those
211 corresponding changes are absent in *fard-1* mutants. Strikingly, phenformin-
212 treated wild type worms display a significant increase in 18:0 DMA versus vehicle,
213 whereas no such increase is evident in drug treated *fard-1* worms (Figure 2C). In
214 addition, relative proportions of stearic acid (18:0) levels within the total fatty acid
215 pool are significantly increased in *fard-1* mutants treated with phenformin versus
216 vehicle treated *fard-1* controls (Figure 2D). In comparison, the relative proportion
217 of stearic acid does not rise in phenformin treated wild type animals, suggesting
218 that stearate is being utilized for ether lipid production. Analysis of the total fatty
219 acid pool by GC-MS (Figure 2—figure supplement 1) indicates that aside from
220 several fatty acids (e.g. 18:2), the most pronounced differences were in the
221 plasmalogen pool. In alignment, an assessment of levels of additional alkenyl fatty
222 alcohols in phenformin-treated, wild type animals indicates a parallel, significant
223 increase in the less abundant 16:0 DMA and 18:1 DMA species (Figure 2E). We
224 conclude that phenformin treatment leads to an overall increase of alkenyl ether
225 lipid levels in *C. elegans*.
226 To investigate relative changes in individual ether lipid abundance in
227 response to phenformin at high resolution, we utilized LC-MS analysis. Using this
228 method, we detected 20 alkyl and alkenyl phosphatidylethanolamine-based ether
229 lipids previously noted to be the most abundant ether lipids in *C. elegans*
230 (Drechsler et al., 2016; Shi et al., 2016) (Figure 2F—G and Supplementary file 2).
231 This analysis indicates that phenformin treatment results in a significant increase

232 **Figure 2**

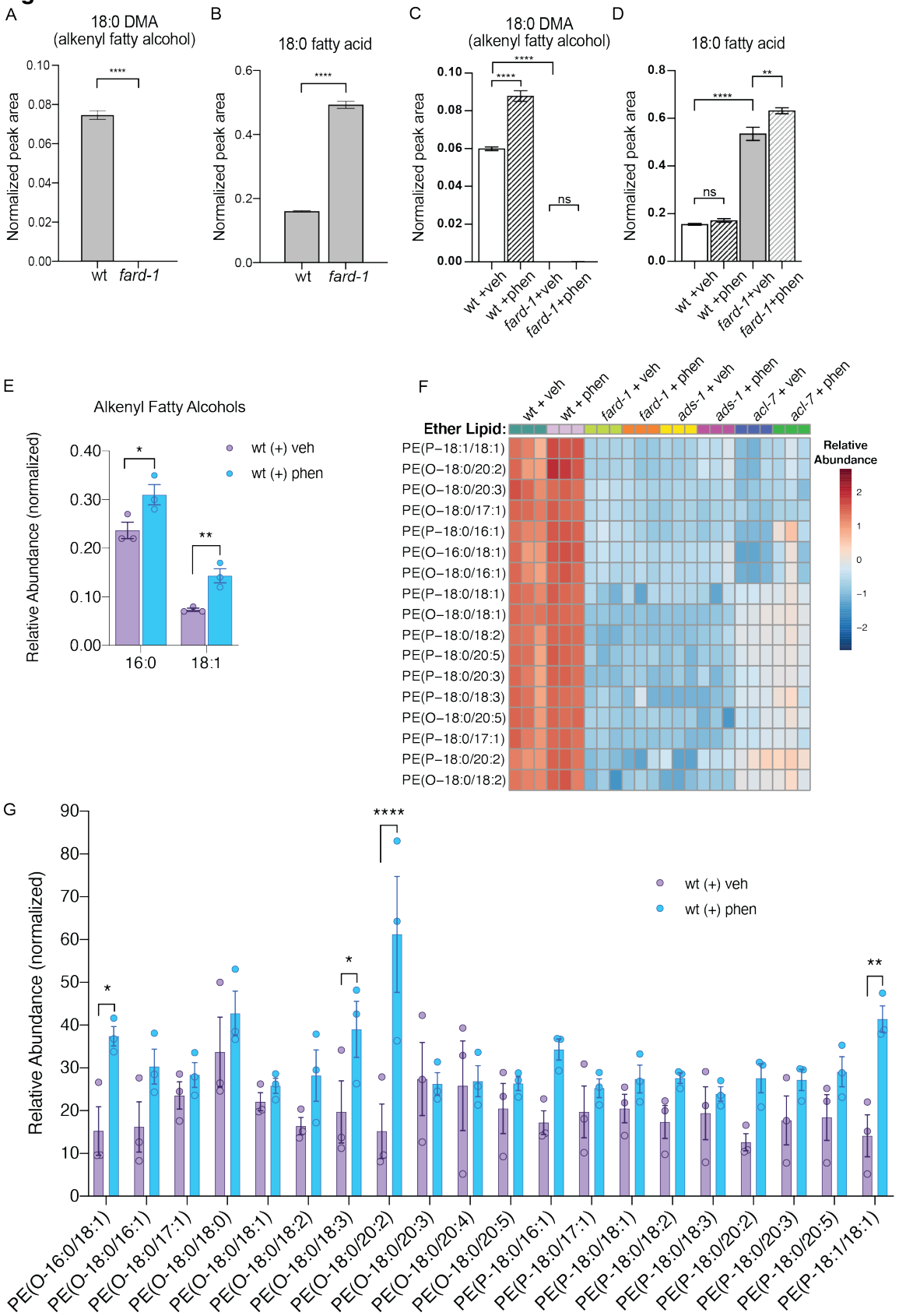
A
18:0 DMA
(alkenyl fatty alcohol)
Normalized peak area
wt
fard-1
B
18:0 fatty acid
C
18:0 DMA
(alkenyl fatty alcohol)
wt +veh
wt +phen
fard-1+veh
fard-1+phen
ns
D
18:0 fatty acid
E
Alkenyl Fatty Alcohols
Relative Abundance (normalized)
wt (+) veh
wt (+) phen
16:0
18:1
F
wt + veh
wt + phen
fard-1 + veh
fard-1 + phen
ads-1 + veh
ads-1 + phen
acl-7 + veh
acl-7 + phen
Ether Lipid:
Relative Abundance
PE(P−18:1/18:1)
PE(O−18:0/20:2)
PE(O−18:0/20:3)
PE(O−18:0/17:1)
PE(P−18:0/16:1)
PE(O−16:0/18:1)
PE(O−18:0/16:1)
PE(P−18:0/18:1)
PE(O−18:0/18:1)
PE(P−18:0/18:2)
PE(P−18:0/20:5)
PE(P−18:0/20:3)
PE(P−18:0/18:3)
PE(O−18:0/20:5)
PE(P−18:0/17:1)
PE(P−18:0/20:2)
PE(O−18:0/18:2)
G
Relative Abundance (normalized)
wt (+) veh
wt (+) phen
PE(O-16:0/18:1)
PE(O-18:0/16:1)
PE(O-18:0/17:1)
PE(O-18:0/18:0)
PE(O-18:0/18:1)
PE(O-18:0/18:2)
PE(O-18:0/18:3)
PE(O-18:0/20:2)
PE(O-18:0/20:3)
PE(O-18:0/20:4)
PE(O-18:0/20:5)
PE(P-18:0/16:1)
PE(P-18:0/17:1)
PE(P-18:0/18:1)
PE(P-18:0/18:2)
PE(P-18:0/18:3)
PE(P-18:0/20:2)
PE(P-18:0/20:3)
PE(P-18:0/20:5)
PE(P-18:1/18:1)

233 **Figure 2. Phenformin treatment of *C. elegans* leads to increased abundance of**
234 **multiple alkyl and alkenyl ether lipids.** (A-B) Loss-of-function *fard-1* mutants have
235 significant reduction in 18:0 fatty alcohols derivatized from 18-carbon containing alkenyl
236 ether lipids (dimethylacetal, DMA) by GC/MS (A) and accumulation of the saturated fatty
237 acid stearate (18:0, B). (C) Wild type worms treated with 4.5 mM phenformin display a
238 significant increase in 18:0 DMA relative to vehicle control, indicative of higher levels of
239 alkenyl ether lipids, with levels remaining essentially undetectable in *fard-1* mutants on
240 vehicle or drug. (D) 4.5mM phenformin treatment does not impact stearate levels in wild
241 type worms, however it does result in a greater accumulation of stearate in *fard-1* mutants.
242 For A-D, **, $P < 0.01$; ****, $P < 0.0001$, by t-test (A-B) or two-way ANOVA (C-D), n = 3
243 biological replicates. (E) 4.5mM phenformin treatment results in a significant increase in
244 16:0 DMA and 18:1 DMA in wild type worms, relative to vehicle-treated controls (*, $P <$
245 0.05; **, $P < 0.01$, by multiple t-tests, with two-stage linear step-up procedure of Benjamini,
246 Krieger and Yekutieli. n = 3 biological replicates. (F) Heat map of normalized ether lipid
247 abundance following phenformin treatment in wild type *C. elegans* indicates an overall
248 increase in ether lipids relative to vehicle treated controls, and this shift is absent in ether
249 lipid deficient mutants. All metabolites shown have an FDR adjusted $P < 0.05$ by one-way
250 ANOVA followed by Fisher's LSD post-hoc testing for WT versus *fard-1*, *ads-1,* and *acl-7*
251 mutants. (G) LC-MS analysis shows that phosphatidylethanolamine-containing ether lipids
252 detected exhibited a general trend towards increased abundance in wild type worms
253 treated with 4.5mM phenformin. Four of these ether lipids reached statistical significance:
254 PE(O-16:0/18:1), PE(O-18:0/18:3), PE(O-18:0/20:2), and PE(P-18:1/18:1). Eleven of the
255 ether lipids detected are of the alkyl-type (indicated by "O" in their name prior to fatty
256 alcohol designation) whereas 9 are of the alkenyl-type (plasmalogen, indicated by "P" in
257 their name prior to the fatty alcohol designation) ether lipids. For *G*, *, $P < 0.05$; **, $P <$
258 0.01; ****, $P < 0.0001$, by multiple t-tests, with multiple hypothesis testing correction by
259 two-stage step-up method of Benjamini, Krieger, and Yekutieli, n = 3 biological replicates.
260 See Supplementary file 2 for raw and normalized mass spectrometry data.

261 in normalized abundance of four ether lipids, PE(O-16:0/18:1), PE(O-18:0/18:3),
262 PE(O-18:0/20:2), and PE(P-18:1/18:1), even when corrected for multiple
263 hypothesis testing. The vast majority of ether lipids measured display mean levels
264 that increase with phenformin treatment, though most are either nominally
265 significant or exhibit a nonsignificant trend because of the strict threshold required
266 to reach significance when correcting for multiple hypotheses. Finally,
267 phosphatidylethanolamine ether lipid abundances were extremely low in *fard-1,*
268 *acl-7* and *ads-1* mutants and unchanged by phenformin treatment, unlike in wild
269 type animals (Figure 2F and Supplementary file 2). In aggregate, these data
270 indicate that phenformin treatment leads to increased abundance of multiple ether
271 lipid species in *C. elegans*.
272
273 **Peroxisomal ether lipid synthesis is essential to phenformin effects**
274 In order to begin to understand the governance of ether lipid biosynthesis by
275 biguanides, we examined expression of a *C. elegans* FARD-1::RFP translational
276 reporter, under the control of its own promoter (Figure 2—figure supplement 2A).
277 Exogenously expressed FARD-1 *(fard-1 oe1)* is expressed in intestine and
278 localizes near structures resembling lipid droplets by Nomarski microscopy (Figure
279 2—figure supplement 2B). Given that ether lipid biogenesis occurs between
280 peroxisomes and the endoplasmic reticulum (ER) (Ghosh and Hajra, 1986;
281 Hardeman and Van den Bosch, 1989; Hua et al., 2017; Singh et al., 1993), we
282 crossed this FARD-1::RFP reporter to an animal bearing a GFP reporter that
283 illuminates peroxisomes in intestine (GFP fused to a C-terminal peroxisomal
284 targeting sequence 1 (PTS1)) to determine if localization of FARD-1 is regulated
285 by biguanides. FARD-1 does not possess a predicted C-terminal PTS1 as do ACL-
286 7 and ADS-1. At baseline, FARD-1::RFP fluorescence partially overlaps with
287 peroxisomally-targeted GFP (Figure 2—figure supplement 2C). Colocalization
288 analysis indicates that treatment with phenformin does not change the amount of
289 overlap between FARD-1::RFP and GFP::PTS1 relative to vehicle treated controls
290 (Figure 2—figure supplement 2D). To confirm our earlier observation that suggests
291 FARD-1 colocalization with lipid droplets, we used confocal imaging to assess the
292 spatial distribution of an integrated FARD-1::RFP reporter *(fard-1 oe3)* in *C.*
293 *elegans* fed C1-BODIPY-C12 to label lipid droplets (and treated with *glo-4* RNAi to
294 remove BODIPY-positive lysosome-related organelles) (Hermann et al., 2005;
295 Zhang et al., 2010a; Zhang et al., 2010b) We found that FARD-1::RFP
296 fluorescence directly surrounds some, but not all, BODIPY-positive lipid droplets
297 in the worm intestine (Figure 2—figure supplement 2E). However, as with
298 peroxisomes, phenformin does not alter the number of lipid droplets that are
299 surrounded by FARD-1 or its distribution around lipid droplets (data not shown.)
300 Finally, FARD-1::RFP localizes into web-like structures in the *fard-1(oe3)* reporter
301 that may represent endoplasmic reticulum versus another cellular tubular vesicular
302 network (Figure 2—figure supplement 2F), and this localization is also not altered
303 by biguanide treatment. Thus, the regulation of ether lipid biosynthesis does not
304 appear to be via differential localization of FARD-1.

305 Expression of mRNAs encoding FARD-1, ACL-7, and ADS-1 are all
306 decreased or unchanged in abundance upon treatment with biguanide via
307 quantitative RT-PCR (Figure 2—figure supplement 2G—L), suggesting that ether
308 lipids are not increased in phenformin treatment through a transcriptional
309 mechanism. A parallel decrease in overall levels of FARD-1::RFP protein of *fard-*
310 *1(oe1)* transgenics was seen with phenformin treatment (Figure 2—figure
311 supplement 2M). These seemingly paradoxical data are likely consistent with post-
312 translational negative feedback of ether lipids on the ether lipid biosynthetic
313 pathway, as has been previously reported.
314 To affirm that the peroxisome is an essential site of ether lipid production in
315 biguanide action, we disrupted peroxisomal protein targeting and examined
316 phenformin-stimulated lifespan extension. Indeed, either *prx-5* or *prx-19* RNAi
317 impair lifespan extension prompted by phenformin fully or partially, respectively
318 (Figure 3A—B). PRX-5 is involved in protein import into the peroxisomal matrix
319 and PRX-19 is involved in proper sorting of proteins for peroxisomal biogenesis.
320 Thus, either disruption of ether lipid biosynthetic machinery or of a principal site of
321 ether lipid biosynthesis impairs phenformin's prolongevity benefit.
322
323 **Fatty acid elongases and desaturases are positive effectors of biguanide-**
324 **mediated lifespan extension**
325 Most mature ether lipid species contain a fatty acid in the *sn-2* position linked by
326 an ester bond (Dean and Lodhi, 2018). The majority of fatty acids conjugated in
327 ether lipids are largely synthesized endogenously in *C. elegans* by fatty acid
328 desaturases and fatty acid elongases (Perez and Van Gilst, 2008; Perez and
329 Watts, 2021) (Figure 3C). Thus, we hypothesized that some of these desaturases
330 and elongases may also contribute mechanistically to biguanide-mediated lifespan
331 extension. Indeed, RNAi knockdown of three fatty acid desaturases and two fatty
332 acid elongases in phenformin-treated *C. elegans* blunted phenformin-stimulated
333 lifespan extension relative to empty vector controls (Figure 3D—H). Notably, these
334 five genes all contribute to the production of fatty acids 18-20 carbons in length
335 with three or more double bonds. Although knockdown of fatty acid desaturases
336 and elongases in *C. elegans* results in inherent lifespan extension on vehicle
337 relative to wild type controls on empty vector RNAi as has been previously reported
338 (Horikawa et al., 2008; Shmookler Reis et al., 2011), these RNAi knockdown either
339 largely (as in the case of *fat-1,* Figure 3D) or completely mitigate phenformin-driven
340 lifespan extension (as in the case of *fat-3, fat-4, elo-1* and *elo-2,* Figure 3E—H).
341 These results suggest the tantalizing possibility that fatty acid desaturases and
342 elongases promote biguanide-mediated lifespan extension through contribution of
343 long and polyunsaturated fatty acids to the synthesis of ether lipids, though a
344 mechanistically distinct role is also possible.

345 **Figure 3**

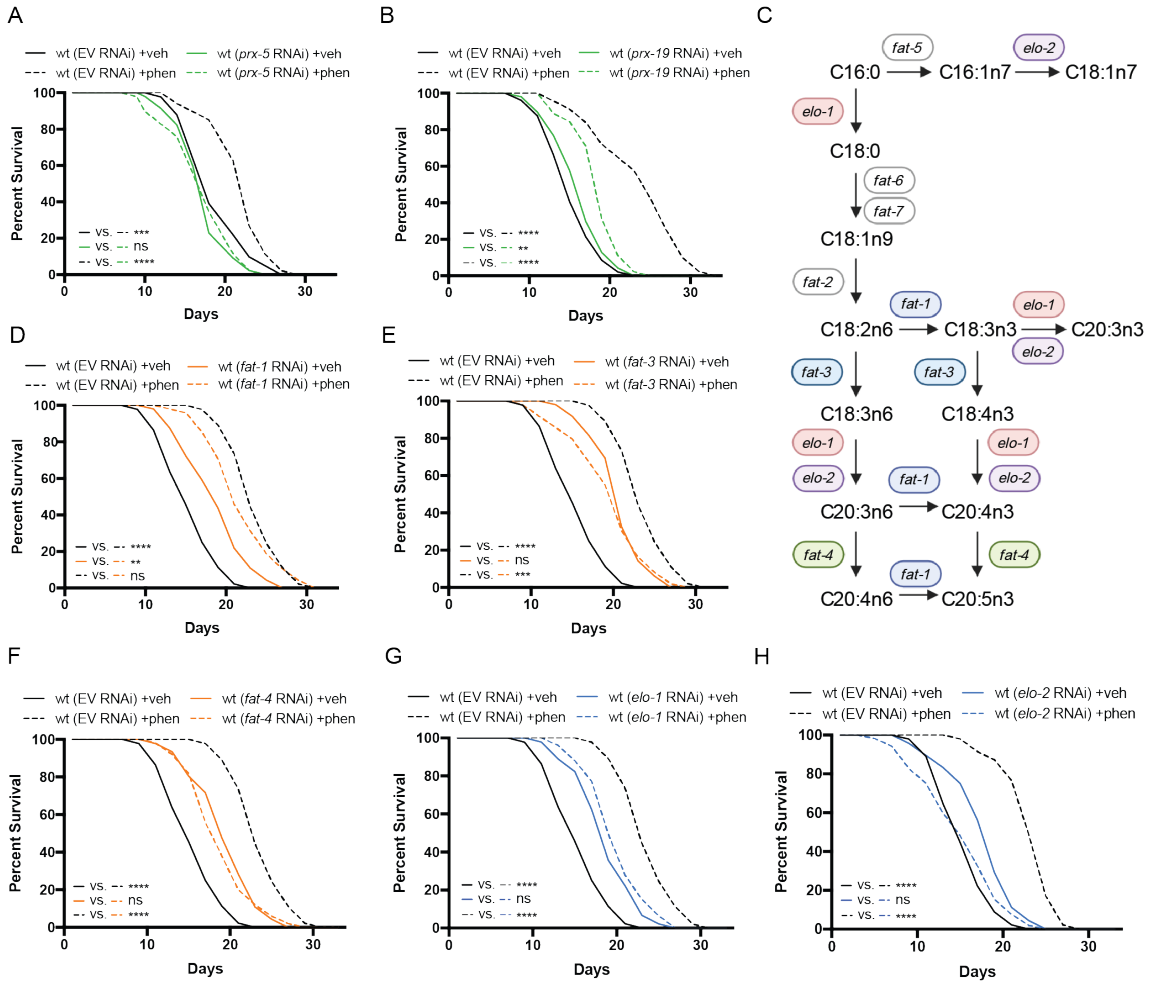

346 **Figure 3. Peroxisomal protein import, fatty acid elongases, and fatty acid**
347 **desaturases are required for the prolongevity effects of biguanides.** (A-B)
348 Knockdown of *prx-5* (A) and *prx-19* (B) by RNAi eliminates or significantly suppresses
349 phenformin-mediated lifespan extension. (C) Schematic representation of the mono-
350 (MUFA) and poly-unsaturated fatty acid (PUFA) synthesis pathway in *C. elegans* (adapted
351 from (Watts, 2016)). (D-H) RNAi of three fatty acid desaturases (D-F) and two fatty acid
352 elongases (G and H) involved in the synthesis of 18- and 20-carbon polyunsaturated fatty
353 acids blunt phenformin-mediated lifespan extension in wild type worms. Colored symbols
354 for *elo* and *fat* genes (vs. those in black and white) in Figure 3C indicates those that inhibit
355 phenformin lifespan extension when knocked down by RNAi. For A, B and D-H, results
356 are representative of 2-3 biological replicates. **, $P < 0.01$; ***, $P < 0.001$; ****, $P < 0.0001$
357 by log-rank analysis; see also Supplementary file 1 for tabular survival data and biological
358 replicates.

359 **Genes involved in ether lipid biosynthesis are required in multiple longevity**
360 **paradigms**
361 Given the critical role of ether lipids in the response to biguanides, we
362 hypothesized that these molecules may also play a broader role in diverse
363 longevity paradigms involving metabolic or nutrient-sensing pathways. *C. elegans*
364 mutant strains that exhibit 1) reduced mitochondrial function (*isp-1*), 2) disrupted
365 mTORC1 signaling (*raga-1*), 3) abnormal pharyngeal pumping (*eat-2*), or 4)
366 inhibition of insulin/insulin-like growth factor-1 signaling (*daf-2*), all result in
367 extension of lifespan (Apfeld et al., 2004; Curtis et al., 2006; Schreiber et al., 2010;
368 Senchuk et al., 2018). To determine whether requirement for the ether lipid
369 biosynthetic machinery in aging generalizes to these other lifespan extension
370 paradigms, we knocked down all three ether lipid biosynthetic enzymes by RNAi
371 in wild type *C. elegans* and four long-lived genetic mutants: *raga-1*, *isp-1*, *eat-2*,
372 and *daf-2*. Knockdown of *fard-1*, *acl-7*, and *ads-1* by RNAi results in suppression
373 of lifespan extension in *isp-1*, *raga-1*, and *eat-2* mutants (Figure 4A—C). However,
374 knockdown of ether lipid synthesis genes by RNAi did not impact lifespan
375 extension in *daf-2* mutants (Figure 4—figure supplement 1A). Thus, the ether lipid
376 biosynthetic machinery plays a broad role in lifespan extension, and, importantly,
377 does not non-selectively shorten lifespan by making animals generally unfit.

378 **Figure 4**

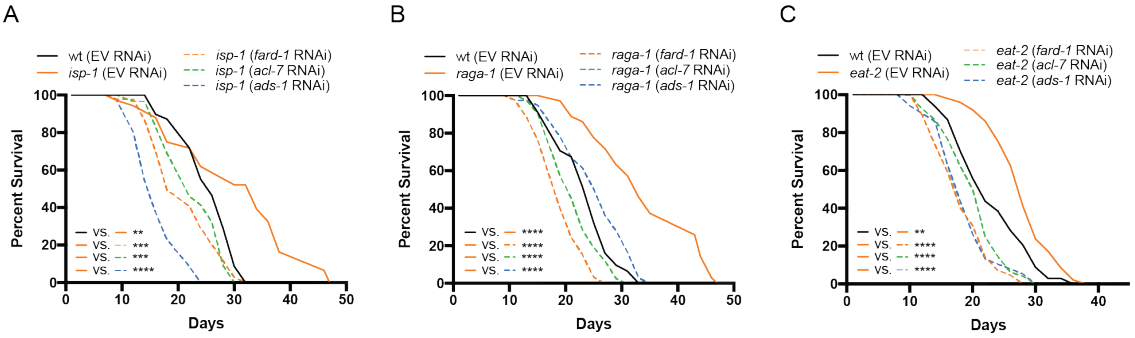

379 **Figure 4. Genes involved in ether lipid biosynthesis are required for lifespan**
380 **extension in multiple longevity paradigms.** (A-C) *isp-1*, *raga-1*, and *eat-2* mutants
381 display extended lifespan relative to wild type animals that is suppressed by RNAi
382 knockdown of any of the three members of the ether lipid biosynthetic pathway. Results
383 are representative of 3 biological replicates. **, $P < 0.01$; ***, $P < 0.001$; ****, $P < 0.0001$
384 by log-rank analysis. See also Figure 4—figure supplement 1 and Supplementary file 1
385 for tabular survival data and biological replicates.

386 **Overexpression of *fard-1* is sufficient to promote lifespan extension**
387 To determine whether stimulation of ether lipid biosynthesis is sufficient to prompt
388 lifespan extension, we tested the effect of overexpression (*oe*) of the sole *C.*
389 *elegans* fatty acid reductase that synthesizes fatty alcohols for ether lipid
390 biogenesis, *fard-1,* on lifespan. Strikingly, *fard-1(oe1)* alone significantly extends
391 lifespan (Figure 5A). This result is similar in a second, independent *fard-1(oe2)*
392 transgenic line (Figure 5B). To confirm that *fard-1(oe)* lifespan extension is
393 dependent upon ether lipid biosynthesis, we knocked down *fard-1*, *acl-7*, and *ads-*
394 *1* by RNAi in the *fard-1(oe1)* transgenic. As predicted, knockdown of three ether
395 lipid biosynthetic enzymes leads to significant suppression of *fard-1(oe1)* lifespan
396 extension (Figure 5C and (Figure 4—figure supplement 1B—C).
397 To determine whether lifespan extension attributable to *fard-1(oe)* shares
398 genetic dependencies with biguanide-mediated longevity, we independently
399 knocked down *skn-1*/*Nrf2*, *aak-2/*AMPK and *daf-16*/*FoxO* by RNAi in a *fard-1(oe)*
400 background. While *skn-1*/*Nrf2* and *aak-2/*AMPK have previously been
401 demonstrated to be necessary for metformin-stimulated lifespan extension, *daf-*
402 *16/FoxO* has not (Kenyon et al., 1993; Onken and Driscoll, 2010). Lifespan
403 extension attributable to *fard-1(oe1)* is suppressed by these three gene
404 knockdowns (Figure 5D—F), indicating that it is mechanistically similar, but not
405 identical, to biguanide-mediated lifespan extension (Cabreiro et al., 2013; Onken
406 and Driscoll, 2010). In aggregate, these results support the notion that ether lipids
407 are an important requirement in multiple, diverse longevity paradigms, and further
408 that *fard-1(oe)* promotes mechanistically-distinct lifespan extension in *C. elegans.*
409 In order to characterize shifts in ether lipids related to prolongevity effects,
410 we performed comparative GC-MS-based fatty acid profiling of our integrated
411 *fard-1(oe)* animals. Levels of 16:0 and 18:1 alkenyl ether lipids (indicated by
412 DMAs on GC-MS analysis), are significantly increased in *fard-1(oe3)* transgenic
413 animals versus wild type worms (Figure 5G). By comparison, 18:0 ether lipids
414 were not increased, indicating that the ether lipid pool has both similarities and
415 differences between *fard-1* overexpression and phenformin treatment**.** Echoing
416 the analysis seen with phenformin treatment, few differences were found in a
417 comparison of the relative abundance of fatty acids within the total lipid pool for
418 *fard-1(oe3)* and wild type worms (Figure 5H). Those exhibiting increases in *fard-*
419 *1(oe)* include the polyunsaturated fatty acids (PUFA) 20:4 arachidonate and 20:5
420 eicosapentaenoate (EPA). This suggests either that PUFAs play a mechanistic
421 role in lifespan extension in *fard-1(oe)* or that they are increased as a
422 consequence of longevity-promoting activity of ether-lipids.

423 **Figure 5**

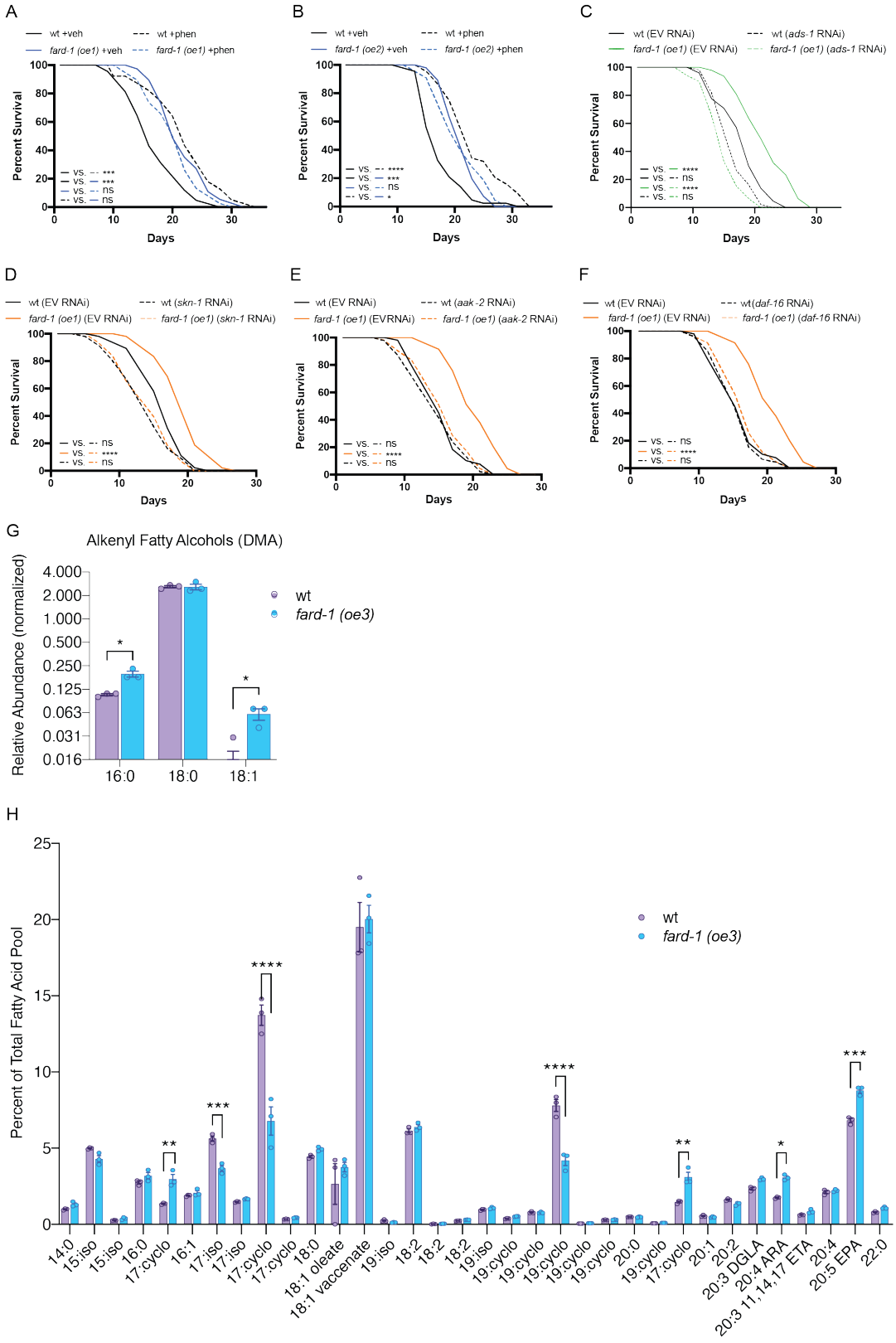
A
wt +veh
wt +phen
fard-1 (oe1) +veh
fard-1 (oe1) +phen
Percent Survival
Days
B
wt +veh
wt +phen
fard-1 (oe2) +veh
fard-1 (oe2) +phen
C
wt (EV RNAi)
wt (ads-1 RNAi)
fard-1 (oe1) (EV RNAi)
fard-1 (oe1) (ads-1 RNAi)
D
wt (EV RNAi)
wt (skn-1 RNAi)
fard-1 (oe1) (EV RNAi)
fard-1 (oe1) (skn-1 RNAi)
E
wt (EV RNAi)
wt (aak-2 RNAi)
fard-1 (oe1) (EVRNAi)
fard-1 (oe1) (aak-2 RNAi)
F
wt (EV RNAi)
wt(daf-16 RNAi)
fard-1 (oe1) (EV RNAi)
fard-1 (oe1) (daf-16 RNAi)
G
Alkenyl Fatty Alcohols (DMA)
Relative Abundance (normalized)
wt
fard-1 (oe3)
16:0
18:0
18:1
H
Percent of Total Fatty Acid Pool
wt
fard-1 (oe3)
14:0
15:iso
15:iso
16:0
17:cyclo
16:1
17:iso
17:iso
17:cyclo
17:cyclo
18:0
18:1 oleate
18:1 vaccenate
19:iso
18:2
18:2
18:2
19:iso
19:cyclo
19:cyclo
19:cyclo
19:cyclo
19:cyclo
20:0
19:cyclo
17:cyclo
20:1
20:2
20:3 DGLA
20:4 ARA
20:3 11,14,17 ETA
20:4
20:5 EPA
22:0

424 **Figure 5. FARD-1 overexpression is sufficient to extend lifespan by modulating**
425 **ether lipid synthesis.** (A-B) Two, independently-generated *fard-1* overexpression *(fard-*
426 *1 oe1 and fard-1 oe2)* transgenic strains exhibit lifespan extension that is not further
427 extended by concomitant phenformin treatment. (C) RNAi knockdown of *ads-1* fully
428 suppresses *fard-1(oe1)* lifespan extension, indicating that the *fard-1(oe)*-mediated
429 lifespan extension is dependent upon ether lipid synthesis. (D-F) RNAi of *skn-1* (D), *aak-*
430 *2* (E), and *daf-16* (F) suppress *fard-1(oe1)*-mediated lifespan extension. For *A-F*, results
431 are representative of 2-3 biological replicates. *, $P < 0.05$; ***, $P < 0.001$; ****, $P < 0.0001$
432 by log-rank analysis. See also Figure 4—figure supplement 1 and Supplementary file 1
433 for tabular survival data and biological replicates. (G) Worms overexpressing integrated
434 FARD-1 *(fard-1 oe3)* display a significant increase in 16:0 and 18:1 but not 18:0 alkenyl
435 ether lipids by GC/MS. (H) Comparison of the total fatty acid pool indicates that the
436 polyunsaturated fatty acids 20:4 arachidonic acid (ARA) and 20:5 eicosapentaenoic acid
437 (EPA) are significantly increased in *fard-1* overexpressing *(fard-1 oe3)* worms vs. wild type
438 animal, while several isomethyl (iso) and cyclopropyl (cyclo) fatty acids change in
439 opposing directions. For *G-H*, n = 3 biological replicates. *, $P < 0.05$; **, $P < 0.01$; ***, P
440 < 0.001; ****, $P < 0.0001$ by multiple t-tests (with multiple hypothesis correction by two-
441 stage step-up method of Benjamini, Krieger, and Yekutieli).

442 **Ether lipids do not promote lifespan extension by modulating ferroptosis**
443 Ether lipids have been reported to be protective against ferroptosis, an iron-
444 dependent form of programmed cell death characterized by the accumulation of
445 lipid peroxides (Perez et al., 2020; Zou et al., 2020). In order to determine whether
446 ether lipids promote longevity downstream of biguanide action by modulating
447 ferroptosis, we knocked down members of the glutathione peroxidase (GPX) family
448 in animals overexpressing integrated *fard-1 (fard-1 oe3* and *fard-1 oe4)*, as has
449 been previously reported to genetically facilitate lipid peroxidation and ferroptosis
450 (Perez et al., 2020; Sakamoto et al., 2014) (Figure 5—figure supplement 1A—C).
451 This analysis indicates that *gpx-1* (ortholog of human GPX4) RNAi leads to
452 variable lifespan extension relative to wild type controls and exhibits non-additive
453 lifespan extension with *fard-1(oe)* (Figure 5—figure supplement 1A). Neither *gpx-*
454 *6* nor *gpx-7* knockdown impacts lifespan extension in *fard-1(oe)* animals (Figure
455 5—figure supplement 1B—C). Further, GPX family RNAi do not negatively impact
456 lifespan extension reproducibly downstream of phenformin (Figure 5—figure
457 supplement 1D—F). We conclude that genetic triggers that induce ferroptosis do
458 not impact phenformin-prompted or *fard-1(oe)* lifespan extension, and thus it is
459 unlikely that either extend lifespan by suppressing ferroptosis.
460
461 **The ether lipid biosynthetic machinery operates upstream of the stress**
462 **responsive factor, *skn-1/Nrf2,* to enable lifespan extension in response to**
463 **biguanides**
464 We noted when analyzing FARD-1 protein localization that somatic lipid droplets
465 are generally less numerous in BODIPY-stained, phenformin-treated animals vs.
466 vehicle. Indeed, quantitative analysis indicates that intestinal lipid droplets are
467 significantly less numerous following phenformin treatment (in *glo-4* RNAi-treated
468 FARD-1::RFP transgenics *(fard-1 oe3)* fed C1-BODIPY-C12 to label lipid droplets,
469 Figure 6A). We previously reported that gain-of-function mutations in the nutrient-
470 and stress-responsive transcription factor *skn-1/Nrf2* prompt age-dependent,
471 somatic depletion of fat (Asdf) (Lynn et al., 2015; Nhan et al., 2019). This, together
472 with early adult decreases in lipid droplet numbers, suggested to us that
473 phenformin may prompt longevity by activating metabolic stress defenses in a *skn-*
474 *1*-dependent manner. Strikingly, we found that phenformin treatment produces
475 Asdf at day three of adulthood, quantitatively analogous to and non-additive with
476 *skn-1* gain-of-function mutants (Figure 6B—C). Compellingly, loss of function
477 mutations in any of the three ether lipid biosynthetic genes completely prevent the
478 phenformin-mediated Asdf phenotype (Figure 6B—C). Together with the
479 observation that promotion of lifespan extension by both phenformin and *fard-1(oe)*
480 require *skn-1,* these data suggest that biguanides activate an ether lipid-*skn-1*
481 signaling relay to drive longevity-associated metabolic shifts.

482 **Figure 6**

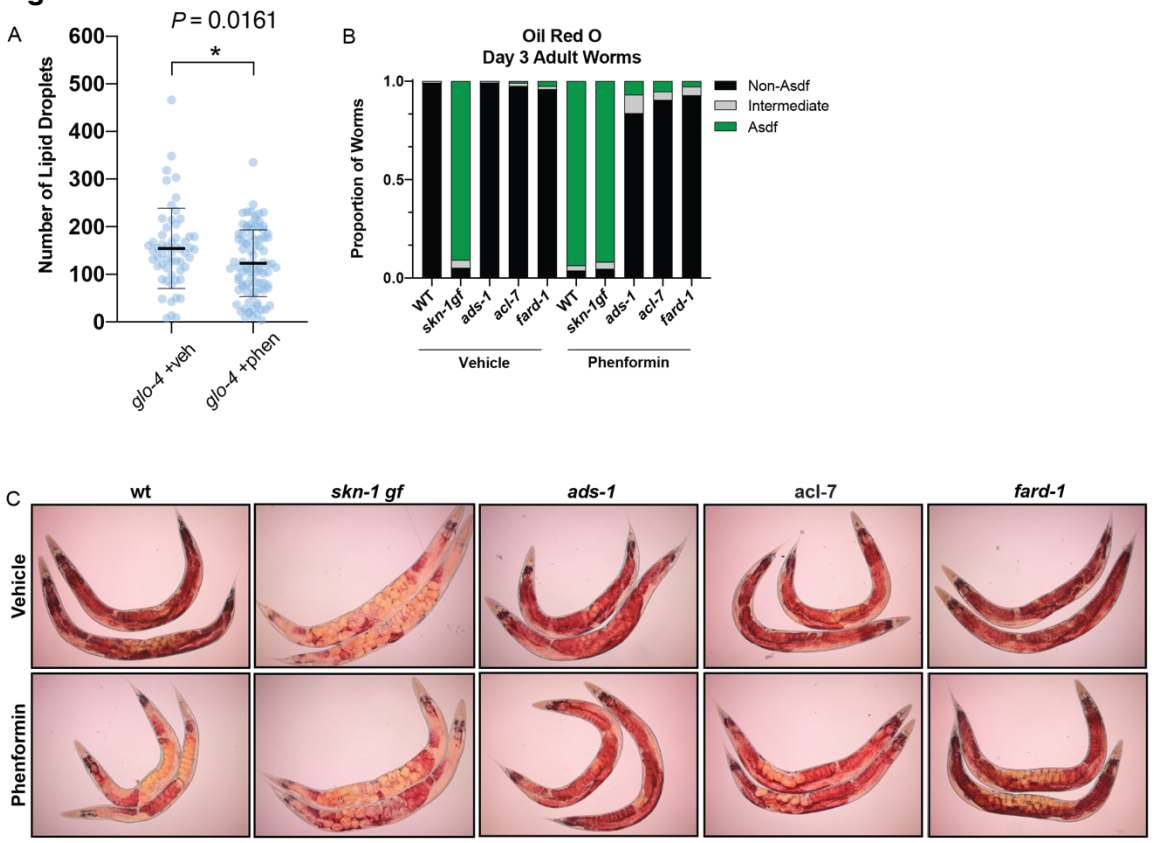

483 **Figure 6. Phenformin modulates systemic lipid metabolism through an ether lipid-**
484 ***skn-1* signaling relay.** (A) The number of intestinal, C1-BODIPY-C12 labeled lipid
485 droplets are significantly lower in phenformin treated animals versus vehicle (FARD-
486 1::RFP reporter transgenic *(fard-1 oe3)* worms are also treated with *glo-4* RNAi to remove
487 BODIPY-positive lysosome-related organelles). n=2 biological replicates. *, $P < 0.05$ by
488 unpaired t-test. (B-C) Oil-red-O staining of day 3 adult phenformin treated wild type
489 animals indicates that drug treatment leads to age-dependent somatic depletion of fat
490 (Asdf), as previously reported for *skn-1* gain of function mutants (*skn-1 gf)*, suggesting
491 that phenformin activates Asdf downstream of *skn-1*. Quantification (B) indicates that the
492 proportion of Asdf animals is non additively increased by phenformin treatment in a *skn-*
493 *1gf* mutant, and that phenformin is no longer able to activate Asdf in 3, independent ether
494 lipid deficient mutants in *ads-1*, *acl-7*, and *fard-1*. For *B-C*, n=3 biological replicates.

Discussion

In an unbiased RNAi screen of ~1000 metabolic genes, we identified ether lipid biosynthesis as critical to the longevity-promoting effects of metformin in *C. elegans*. Our results show that the biguanides metformin and phenformin promote lifespan extension by stimulating biogenesis of ether lipids, prompting longevity-promoting, metabolic stress defenses mediated by *skn-1*. The broad importance of ether lipids is demonstrated by their requirement in multiple, diverse paradigms of lifespan extension. Our findings also indicate that ether lipid modulation through overexpression of *fard-1* is also sufficient to promote longevity. Thus, ether lipids form a heretofore unappreciated lynchpin of lifespan modulation, and are sufficient to support healthy aging through multiple, central longevity effectors, including *skn-1*.

Differences in ether lipid abundance and composition are correlated with diseases of aging. The uniform lethality associated with human genetic ether lipid deficiency, as in the case of patients diagnosed with RCDP and Zellweger syndrome, has made it difficult to study the role of ether lipids in aging and aging-associated diseases (Braverman et al., 1997; Itzkovitz et al., 2012; Motley et al., 1997; Purdue et al., 1997). Nonetheless, observational studies demonstrate decreases in certain plasmalogen species in Alzheimer's Disease, suggesting a probable link between ether lipids and aging-related pathologies (Goodenowe et al., 2007; Grimm et al., 2011; Han et al., 2001). Ether lipids have conflicting roles in cancer; while loss of the ether lipid biosynthetic machinery profits cancer cell survival by enhancing resistance to ferroptosis (Zou et al., 2020), in other contexts, ether lipid deficiency results in impaired pathogenicity in various human cancer cells (Benjamin et al., 2013; Perez et al., 2020). Cancer cells generally have higher levels of ether lipids compared to normal cells, leading others to suggest that ether lipids confer pro-survival benefit (Albert and Anderson, 1977; Benjamin et al., 2013; Snyder and Wood, 1969). However, certain ether lipid species have also been reported to have anti-tumor properties (Arthur and Bittman, 2014; Jaffrès et al., 2016). Thus, in line with the results we present here, it is critical to understand ether lipids in context. Future work will need to focus on the impact of specific ether lipid species rather than the whole class *en masse* to understand which may play a beneficial versus detrimental role in health.

Studies in long-lived animal models suggest there is an association between ether lipid content and animal longevity, such as in the naked mole-rat (*Heterocephalus glaber*) (Mitchell et al., 2007) and the mud clam *Arctica islandica* (Munro and Blier, 2012). Higher plasmalogen levels in naked mole-rat tissues versus mice are speculated to contribute to protection of cellular membranes via a reduction of oxidative stress (Mitchell et al., 2007). Similarly, exceptionally long-lived humans harbor higher levels of phosphatidylcholine-derived, short chained alkyl ether lipids and a lower levels of phosphatidylethanolamine-derived longer chained plasmalogens (Pradas et al., 2019), but these associations are of unclear

538 functional significance. Although it is clear that ether lipid deficiency in *C. elegans*
539 prevents longevity downstream of mitochondrial electron transport chain
540 dysfunction, mTOR deficiency, caloric restriction, and biguanides alike, the precise
541 lipid(s) conferring this activity remains unknown. Each of these longevity
542 paradigms have features of nutrient deficiency, energy stress, or nutrient sensing,
543 so it is possible that ether lipids are at least part of the common effector arm
544 conferring benefit in aging to various forms of metabolic stress.
545 Our results suggest that unsaturated fatty acids and
546 phosphatidylethanolamine ether lipids are essential to the health promoting effects
547 of biguanides. Although we see major shifts in abundance of alkenyl ether lipids,
548 genetic evidence of necessity of ether lipids, and requirement for the synthesis of
549 mono- and poly-unsaturated fatty acids in biguanide-induced longevity,
550 determination of the specific lipids necessary for promoting healthy aging awaits
551 the ability to modulate the level of specific ether lipids. Additionally, disruption of
552 ether lipid biosynthesis has been shown to increase the proportion of stearate
553 (18:0) and other saturated fatty acids (Shi et al., 2016). Thus, at this time, we
554 cannot rule out the possibility that biguanide-stimulated alterations in ether lipid
555 biosynthesis serves to divert accumulation of lipid species that are detrimental to
556 lifespan, for instance, saturated fatty acids. Nonetheless, in light of our finding that
557 ether lipids prompt metabolic stress defenses, this alternative mechanism is less
558 likely. Definitive proof will require a deeper understanding of the regulation of
559 specific steps dictating the synthesis and modification of ether lipids of different
560 fatty alcohol and fatty acid composition.
561 Based upon our findings, ether lipid synthesis is likely to be regulated post-
562 translationally by biguanide treatment. The demonstrated increase in
563 plasmalogens and specific ether lipids are both consistent with increases in activity
564 of the ether lipid biosynthetic machinery. While we do not understand the
565 mechanism for the increased activity of ether lipid synthesizing enzymes, the
566 decreases in mRNAs for *acl-7*, *ads-1*, and *fard-1* and protein for FARD-1 invokes
567 negative feedback consistent with previous work showing that higher levels of
568 ether lipids promotes proteasomal degradation of peroxisomal Far1 protein
569 (Honsho et al., 2010). Co-localization of the fatty alcohol reductase, FARD-1, with
570 both peroxisomes and lipid droplets is similarly not impacted by biguanides.
571 Further investigation into the precise molecular interactions between FARD-1
572 protein and other organelles will be required to further understand how FARD-1
573 and the other ether lipid biosynthetic enzymes are regulated by biguanides and in
574 aging.
575 Strikingly, our data demonstrate for the first time that ether lipids are
576 required for phenformin to activate metabolic defenses downstream of the stress-
577 and metabolism-responsive transcription factor *skn-1*/NRF2. Phenformin drives
578 age-dependent somatic depletion of fat (Asdf), a phenotype we previously reported
579 upon genetic activation of *skn-1* (Lynn et al., 2015; Nhan et al., 2019). Based upon
580 the work of others and our own unpublished work, biguanides do not potentially
581 stimulate canonical *skn-1* antioxidant defenses such as *gst-4* expression (Cabreiro

582 et al., 2013; Onken and Driscoll, 2010). We suggest that *skn-1* is uniquely required
583 for metabolic stress defenses downstream of metformin such as Asdf rather than
584 canonical oxidative or proteostatic defenses. The requirement for ether lipids in
585 Asdf activation by phenformin confirm that this class of lipids plays a heretofore
586 unappreciated role in a distinct form of *skn-1* activation mimicked by genetic forms
587 of *skn-1* activation we have previously reported (Lynn et al., 2015; Nhan et al.,
588 2019).

589 In aggregate, data presented here indicate that ether lipid biosynthesis
590 plays a broader role in aging than previously described. The necessity of the ether
591 lipid machinery in metformin- and phenformin-stimulated lifespan extension and in
592 multiple longevity paradigms indicates that ether lipids serve as a lynchpin through
593 which lifespan is modulated (Figure 7A—B). Our demonstration that
594 overexpression of FARD-1 alone results in lifespan extension provides an exciting
595 opportunity to identify ether lipids that promote health and the effector mechanisms
596 through which they act. Finally, these results support the exciting possibility that
597 modulation of ether lipids pharmacologically or even dietarily may provide a new
598 potential therapeutic target in aging and aging-related diseases.

599 **Figure 7**

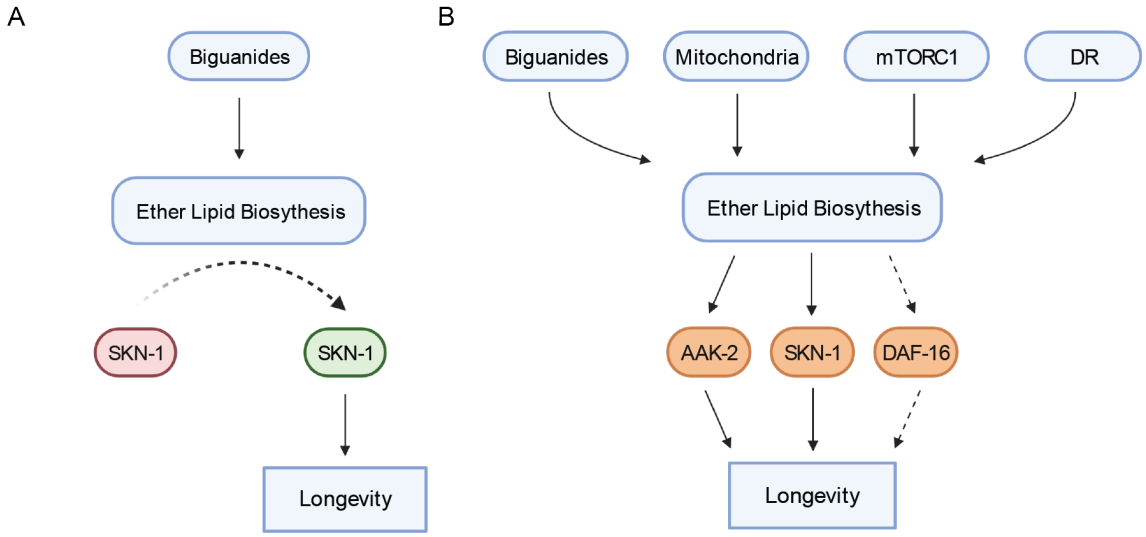

600 **Figure 7. Schematic representation for the role of the ether lipid biosynthetic**
601 **machinery in multiple prolongevity paradigms.** (A) Model of ether lipid action in
602 biguanide-prompted lifespan extension. Activation of ether lipid biosynthesis leads to
603 longevity-promoting activity of metabolic stress defenses downstream of the transcription
604 factor *skn-1*. (B) Model portraying a broader than previously appreciated role of ether lipids
605 in longevity downstream of biguanides, mitochondrial electron transport inhibition,
606 mTORC1 inhibition, and dietary restriction (DR).

607 **Materials and Methods**
608
609 ***C. elegans* genetics.** Strains were maintained at 20°C grown on E. coli OP50-1
610 (RRID: WB-STRAIN:WBStrain00041971) for all experiments unless otherwise
611 indicated. The following strains were used in this study: N2 (wild type strain,
612 RRID: WB-STRAIN:WBStrain00000001), BX275 *fard-1(wa28)* (RRID: WB-
613 STRAIN:WBStrain00004025), BX259 *acl-7(wa20*) (RRID: WS-STRAIN:
614 WBStrain00004024), BX10 *ads-1(wa3*) (RRID: WB-
615 STRAIN:WBStrain00004007), CB1370 *daf-2(e1370*) (RRID: WB-STRAIN:
616 WBStrain00004309), MQ989 *isp-1(qm150*) (RRID: WB-STRAIN:
617 WBStrain00026672), VC533 *raga-1(ok701*) (RRID: WB-STRAIN:
618 WBStrain00035849), DA465 *eat-2(da465*) (RRID:WB-STRAIN:
619 WBStrain00005463), MGH48 *mgIs43*[*ges-1p*::GFP::PTS1], SPC168 *skn-*
620 *1*(*lax188*) (*skn-1gf*, RRID: WB-STRAIN: WBStrain00034420). For *fard-1*
621 overexpression, the following strains were generated: MGH471 *alxEx122*[*fard-*
622 *1p*::FARD-1::mRFP::HA unc-54 3'UTR *myo-2p*::GFP] *(fard-1 oe1)*, MGH472
623 *alxEx135*[*fard-1p*::FARD-1::mRFP::HA unc-54 3'UTR *myo-2p*::GFP] *(fard-1 oe2)*,
624 MGH605 *alxIs45*[*fard-1p*::FARD-1::mRFP::HA::unc-54 3'UTR *myo-2p*::GFP]
625 *(fard-1 oe3)*, and MGH606 *alxIs46*[*fard-1p*::FARD-1::mRFP::HA::unc-54 3'UTR
626 *myo-2p*::GFP] *(fard-1 oe4).* All strains for *fard-1* overexpression were
627 backcrossed 8x to N2 Bristol. For colocalization analysis with peroxisomally
628 targeted GFP, we crossed MGH48 and MGH471 to generate the strain: MGH607
629 *mgIs43*[*ges-1p*::GFP::PTS1]; *alxEx122*[*fard-1p*::FARD-1::mRFP::HA::unc-54
630 3'UTR *myo-2p*::GFP] (noted in text as GFP::PTS1; FARD-1::RFP).

631 **Generation of *fard-1 C. elegans* transgenic lines.** For FARD-1 expression, the
632 entire genomic sequence of the *fard-1* locus (3659 bp), including introns and
633 exons, plus 4910 bp of promoter were amplified and cloned into a modified Fire
634 vector driving *fard-1* fused to mRFP and a HA epitope tag at the C-terminus. The
635 following cloning primers were used:
636
637 F: 5'-TGCATGCCTGCAGGTCGACTTTGACAAAAGTTCTGTTGCCG-3' and
638 R:
639 5'-TTTGGGTCCTTTGGCCAATCGCTTTTTTGAAGATACCGAGAATAATCC-3'.
640
641 The FARD-1 overexpression construct was injected at 10 ng/µL (*alxEx122*) and
642 18 ng/µL (*alxEx135*) into the gonad of wild type adult animals with salmon sperm
643 DNA as a carrier and 1.5 ng/µL *myo-2p*::GFP as a co-injection marker. *alxEx122*
644 was subsequently integrated by UV irradiation and 8x backcrossed to N2 Bristol to
645 obtain MGH605 and MGH606.
646
647 **RNA interference (RNAi) assays.** RNAi clones were isolated from a genome-

648 wide *E. coli* RNAi library (generated in strain HT115(DE3), RRID: WB-
649 STRAIN:WBStrain00041079), sequence verified, and fed to animals as described
650 (Kamath and Ahringer, 2003). RNAi feeding plates (6 cm) were prepared using a
651 standard NGM recipe with 5 mM isopropyl-B–D-thiogalactopyranoside and 200
652 µg/ml carbenicillin. RNAi clones were grown for 15 hours in Luria Broth (LB)
653 containing 100 µg/ml carbenicillin with shaking at 37°C. The stationary phase
654 culture was then collected, concentrated through centrifugation, the supernatant
655 was discarded, and the pellet was resuspended in LB to 20% of the original culture
656 volume; 250 µl of each RNAi clone concentrate was added to RNAi plates and
657 allowed to dry at least 24 hours prior to adding biguanide. Drug treatment was
658 added to seeded RNAi plates and allowed to dry at least 3 hours before adding
659 worms.
660
661 **Longevity assays.** Lifespan analysis was conducted at 20°C, as previously
662 described (Soukas et al., 2009). Briefly, synchronized L1 animals were seeded
663 onto NGM (for mutant treatment) or RNAi plates (for RNAi) and allowed to grow
664 until the L4 to YA transition stage. On day 0 of adulthood as indexed in the figure
665 legend, ~50-60 L4/YA worms per plate (unless otherwise noted) were transferred
666 onto fresh NGM or RNAi plates. These NGM and RNAi plates were supplemented
667 with 30 µM and 100 µM 5-fluorodeoxyuridine (FUdR) to suppress progeny
668 production, respectively. For biguanide treatment, about ~55-60 synchronized L1
669 animals (unless otherwise noted) were seeded onto plates containing 50 mM
670 metformin or 4.5 mM phenformin. Based upon power calculation for log-rank
671 analysis, minimum N of 50 (per group) was chosen to satisfy $\alpha = 0.05$, $\beta = 0.2$, and
672 effect size = 20% difference in lifespan (Petrascheck and Miller, 2017). At the
673 L4/YA stage, these worms were transferred to plates containing biguanide
674 treatment and FUdR for the remainder of their life. Dead worms were counted
675 every other day, and scoring investigators were blinded as to the experimental
676 group/treatment until the conclusion of each experiment. Statistical analysis was
677 performed with online OASIS2 resources (Han et al., 2016).

678 **Body Size Determination of *C. elegans*.** We measured worm body size in
679 response to biguanide treatment by imaging as previously described (Wu et al.,
680 2016). Egg prep synchronized wild type worms were treated with empty vector
681 (L4440) or ether lipid biosynthesis machinery RNAi and treated with vehicle
682 (ddH_2O) or 160mM metformin. After ~65-70 hours, worms were transferred into a
683 96 well plate, washed 3x with M9, and paralyzed in M9 buffer with 1 mg/ml
684 levamisole (L9756-10G, Sigma-Aldrich). Once immobilized, brightfield imaging
685 was performed at 5X magnification on a Leica DM6000 microscope within 5
686 minutes of transferring to a 96 well Teflon imaging slide. We determined the
687 maximal, longitudinal cross-sectional area of the imaged worms by using
688 MetaMorph software for a minimum of ~80 animals per condition in each
689 experiment. Results of a single experiment is shown. Each experiment was
690 performed at least twice, and results were consistent between experiments.
691
692 **GC/MS lipidomics.** Lipid extraction and GC/MS of extracted, acid-methanol-
693 derivatized lipids was performed as described previously (Pino and Soukas, 2020;
694 Pino et al., 2013). Briefly, 5000 synchronous mid-L4 animals were sonicated with
695 a probe sonicator on high intensity in a microfuge tube in 100-250 microliters total
696 volume. Following sonication, lipids were extracted in 3:1 methanol: methylene
697 chloride following the addition of acetyl chloride in sealed borosilicate glass tubes,
698 which were then incubated in a 75°C water bath for 1 hour. Derivatized fatty acids
699 and fatty alcohols were neutralized with 7% potassium carbonate, extracted with
700 hexane, and washed with acetonitrile prior to evaporation under nitrogen. Lipids
701 were resuspended in 200 microliters of hexane and analyzed on an Agilent GC/MS
702 equipped with a Supelcowax-10 column as previously described (Pino and
703 Soukas, 2020). Fatty acids and alcohols are indicated as the normalized peak area
704 of the total of derivatized fatty acids and alcohols detected in the sample. Based
705 upon power calculation for pairwise comparison, a minimum N of 3 biological
706 replicates (per group) was chosen to satisfy $\alpha = 0.05$, $\beta = 0.2$, and effect size =
707 50% with $\sigma = 20\%$. Analyses were blinded to the investigator conducting the
708 experiment and mass spectrometry calculations until the conclusion of each
709 experiment when aggregate statistics were computed.
710
711 **LC/MS-MS lipidomics.** Wild type, *fard-1*, *acl-7*, and *ads-1* worm mutants were
712 collected using conditions that enabled our reported longevity phenotypes. Briefly,
713 collection for LC/MS-MS processing comprised of 3 replicates of these 4 strains
714 that were independently treated with vehicle (ddH_2O) and 4.5mM phenformin on
715 10cm NGM plates. Based upon power calculations, as for GC/MS, a minimum N
716 of 3 biological replicates (per group) was chosen to satisfy $\alpha = 0.05$, $\beta = 0.2$, and
717 effect size = 50% with $\sigma = 20\%$, though the power is only expected to hold for the
718 first significant difference detected. Analyses were blinded to the investigator
719 conducting the experiment and mass spectrometry calculations until the
720 conclusion of each experiment when aggregate statistics were computed. A total
721 of ~6,000 animals (2 x 10cmM plates, 3,000 worms per plate) were utilized per

722 sample. These worms were washed with M9 (4x), concentrated into 200 µL of M9,
723 and then flash frozen with liquid nitrogen in 1.5mL Eppendorf microcentrifuge
724 tubes. Worm pellets were transferred to 2 mL impact resistant homogenization
725 tubes containing 300 mg of 1 mm zirconium beads and 1 mL of 90:10
726 ethanol:water. Using a Precellys 24 tissue homogenizer, samples were
727 homogenized in three 10 second cycles at 6400 Hz followed by 2 minutes of
728 sonication. Samples were then placed at -20 °C for one hour to facilitate protein
729 precipitation. Samples were transferred to 1.5 mL microfuge tubes and centrifuged
730 at 14,000 g for 10 minutes at 4 °C. After centrifugation, 120 µL of supernatant was
731 dried *in vacuo* and resuspended in 120 µL of 80:20 methanol:water containing
732 internal standards 1 ng/µL CUDA and 1 ng/µL MAPCHO-12-d38. Lipidomic data
733 was acquired by injecting 20 µL of sample onto a Phenomenex Kinetex F5 2.6 µm
734 (2.1 x 100 mm) column at 40 °C and flowing at 0.35 mL/min. Metabolites were
735 eluted using (A) water containing 0.1% formic acid and (B) acetonitrile:isopropanol
736 (50:50) containing 0.1% formic acid using the following gradient: 0% B from 0-1
737 min, 0-50% B from 1-6 mins, 50-100% B from 6 to 17 minutes and 100% B hold
738 from 17- 20 mins. Compounds were detected using a Thermo Scientific QExactive
739 Orbitrap mass spectrometer equipped with a heated electrospray ionization (HESI)
740 source operating in positive and negative ion mode with the following source
741 parameters: sheath gas flow of 40 units, aux gas flow of 15 units, sweep gas flow
742 of 2 units, spray voltage of +/-3.5 kV, capillary temperature of 265°C, aux gas temp
743 of 350°C, S-lens RF at 45. Data was collected using an MS1 scan event followed
744 by 4 DDA scan events using an isolation window of 1.0 m/z and a normalized
745 collision energy of 30 arbitrary units. For MS1 scan events, scan range of m/z 100-
746 1500, mass resolution of 17.5k, AGC of $1e^6$ and inject time of 50 ms was used. For
747 tandem MS acquisition, mass resolution of 17.5 k, AGC $5e^5$ and inject time of 80
748 ms was used. Data was collected using Thermo Xcalibur software (version
749 4.1.31.9) and analyzed using Thermo QualBrowser (version 4.1.31.9) as well as
750 MZmine 2.36.
751
752 **Statistical analysis of metabolomics data.** All visualization and significance
753 testing of metabolomics was conducted using the MetaboAnalyst 5.0 package
754 (Pang et al., 2021). Mass integration values for 9,192 compounds were extracted
755 from full-scan LC-MS/MS measurements of L4 to young adult (YA) transition wild
756 type (N2 Bristol), *ads-1(wa3)*, *acl-7(wa20)*, and *fard-1(wa28)* animals treated
757 from L1 hatch with vehicle, 4.5 mM phenformin, or 50mM metformin. Missing and
758 zero values in the data matrix were imputed via replacement with 1/5th of the
759 minimum positive value for each variable. Abundance values were subsequently
760 filtered based on interquartile range (reducing the compound list to the 2500
761 most variable compounds), and $\log_{10}$ transformed. Quantile normalization was
762 then performed, followed with division by the standard deviation of each variable
763 (auto-scaling). Normalized abundance values for were then extracted based
764 upon MS/MS signatures for phosphatidylethanolamine ether lipids and assessed
765 for statistical significance via one-way ANOVA followed by false discovery rate

766 (FDR) control using the Benjamini-Hochberg (BH) method (Benjamini and
767 Hochberg, 1995). Post-hoc testing was then performed using Fisher's LSD to
768 evaluate pairwise comparison significance. Metabolites were considered
769 differentially abundant in any one condition with an FDR controlled P value <
770 0.05. The top 25 metabolites across treatment (ranked by ANOVA f statistic and
771 FDR value) were visualized using a heatmap of Euclidean distance
772 measurements, with Ward clustering of samples and normalized compound
773 abundances included. All mass integration values for identified
774 phosphatidylethanolamine containing ether lipids, normalized abundance values,
775 and log-transformed, normalized abundance values, are included in this
776 manuscript as Supplementary file 2.
777
778 **Quantitative RT-PCR.** To assess changes in mRNA levels of *fard-1*, *acl-7*, and
779 *ads-1* in response to biguanide treatment, we used quantitative RT-PCR as
780 previously described (Wu et al., 2016). Briefly, synchronized wild type (N2) L1
781 animals were seeded onto OP50, NGM plates containing vehicle (ddH_2O), 50 mM
782 metformin, or 4.5 mM phenformin. ~1600 worms were collected from 4 6cm plates
783 per replicate, per condition (with no more than 400 worms seeded per plate to
784 prevent overcrowding). n = 3 biological replicates. Worms were collected at the L4
785 to YA transition using M9 buffer and washed an additional 3X, allowing worms to
786 settle by gravity between washes. Total RNA was extracted using TRIzol. Reverse
787 transcription was performed with the Quantitect reverse transcription kit (Qiagen).
788 qRT-PCR was conducted in triplicate using Quantitect SYBR Green PCR reagent
789 (Qiagen) following manufacturer instructions on a Bio-Rad CFX96 Real-Time PCR
790 system (Bio-Rad). If not processed immediately, worms were flash frozen in liquid
791 nitrogen and kept in –80 °C until RNA preparation. The sequences for primer sets
792 used in *C. elegans* are:
793
794 *act-1*:
795 F: 5'-TGCTGATCGTATGCAGAAGG-3' and
796 R: 5'-TAGATCCTCCGATCCAGACG-3'
797
798 *fard-1*:
799 F: 5'-ACAAGTCACCAATGGCTCCAC-3' and
800 R: 5'-GCTTTGGTCAGAGTGTAGGTG-3'
801 *acl-7*:
802 F: 5'-GTTTATGGCTGGCGTGTTG-3' and
803 R: 5'-CGGAGAAGACAGCCCAGTAG-3'
804
805 *ads-1*:
806 F: 5'-GCGATTAACAAGGACGGACA-3' and
807 R: 5'-CGATGCCCAAGTAGTTCTCG-3'.
808

809 Expression levels of tested genes were presented as normalized fold changes to
810 the mRNA abundance of *act-1* for *C. elegans* by the ΔΔCt method.
811
812 **FARD-1 overexpression reporter fluorescence intensity analysis.** To assess
813 changes in levels of fluorescent FARD-1 protein in response to biguanide
814 treatment, we used the strain MGH471 *alxEx122*[*fard-1p*::FARD-1::mRFP::HA
815 unc-54 3'UTR *myo-2p*::GFP] *(fard-1 oe1)*. In brief, egg prep synchronized L1
816 FARD-1::RFP transgenic worms were treated with vehicle (ddH_2O) or 4.5 mM
817 phenformin, paralyzed with 1 mg/ml of levamisole, and then imaged in 96-well
818 format with a Leica DM6000 microscope outfitted with a mCherry filter set and
819 MMAF software. These imaging experiments were carried out in biological
820 triplicate with ~10 animals imaged per replicate. Images were qualitatively
821 assessed to obtain conclusions and results were consistent between independent
822 replicates.
823
824 **Colocalization analysis of FARD-1::RFP and peroxisomally targeted GFP**
825 Colocalization of GFP and RFP expression in vehicle or phenformin treated
826 MGH607 was performed by Coloc2 (Fiji) on images taken on a Leica Thunder
827 microscopy system. Since FARD-1::RFP in MGH607 is exogenously expressed,
828 we performed 3 hour egg lays with ~30 gravid hermaphrodites expressing both
829 GFP::PTS1 and FARD-1::RFP to synchronize L1s. The eggs were treated with
830 vehicle (ddH_2O) or 4.5mM phenformin immediately after gravid hermaphrodites
831 were removed, dried in a laminar flow hood, and allowed to incubate at 20°C until
832 the worms were young adult/early day 1 adults. To prepare for imaging, only
833 worms expressing both GFP::PTS1 and FARD-1::RFP were picked onto slides
834 containing dried 2% agar pads, immobilized in ~5 µL of 2.5mM levamisole solution
835 and covered with a cover slip. Images of the upper, mid, and lower intestine were
836 taken for 30 individual worms per condition (15 worms per replicate for 2 biological
837 replicates). We generated Pearson's r values to assess the extent to which
838 intestinal RFP and GFP overlap in each region of all samples. All Pearson's r
839 values were combined to generate 4 individual averages (1 per condition) to
840 perform an unpaired t-test.
841
842 **Lipid droplet analysis.** The strain MGH605 *alxIs45*[*fard-1p*::FARD-1::mRFP
843 ::HA::unc-54 3'UTR *myo-2p*::GFP] *(fard-1 oe3)* was used for this analysis.
844 Preparation of worms for imaging was similar to our longevity assays but modified
845 to incorporate staining of lipid droplets. Briefly, 6cm RNAi plates were seeded with
846 250µL bacteria expressing *glo-4* RNAi [5X] and allowed to incubate for 24 hours
847 at 20°C. 1µM of green C1-BODIPY-C12 (D-3823, Invitrogen) diluted in 100µL 1X
848 phosphate buffer saline (PBS, pH 7.2) was then added to the RNAi bacteria lawn
849 as in (Soukas et al., 2009).The plates were immediately dried in a dark laminar
850 flow hood, wrapped in aluminum foil to prevent photobleaching, and allowed to
851 incubate at 20°C for 24-48 hours. These plates were treated with vehicle (ddH_2O)
852 or 4.5mM phenformin as mentioned previously (while kept away from light.) Egg

853 prep synchronized worms were dropped onto plates and grown to day 1 adult
854 stage. To prepare for confocal imaging, animals were rapidly picked onto slides
855 containing dried 2% agar pads, immobilized in ~5 µL of 2.5mM levamisole solution
856 and covered with a cover slip. Lipid droplets were imaged by Zeiss LSM 800
857 Airyscan within 5 minutes of slide placement. Z-stacked images were obtained for
858 the intestine near the tail end of 14 *glo-4,* vehicle treated and 19 *glo-4*, phenformin
859 treated worms (2 biological replicates per condition). 5 planes were extracted
860 (planes 1,2,4,5, and 9) using ImageJ for all samples. For lipid droplet counting,
861 quantification was performed using CellProfiler 4.2.1 (Stirling et al., 2021) where
862 lipid droplets were identified as primary objects. The min/max range for typical
863 object diameters was 3-67 pixels, and those objects outside of the diameter range
864 were discarded. Planes were excluded entirely if the pipeline did not accurately
865 capture individual lipid droplets for the vast majority of objects.
866
867 **Oil Red O Staining.** Oil red O (ORO) fat staining was conducted as outlined in
868 (Stuhr et al., 2022), In brief, worms were egg prepped and allowed to hatch
869 overnight for a synchronous L1 population. The next day, worms were dropped
870 onto plates seeded with bacteria with or without phenformin and raised to 120
871 hours (day 3 adult stage). Worms were washed off plates with PBST, then rocked
872 for 3 min in 40% isopropyl alcohol before being pelleted and treated with ORO in
873 diH2O for 2 hours. Worms were pelleted after 2 hours and washed in PBST for 30
874 min before being imaged at 5x magnification with the DIC filter on the Zeiss Axio
875 Imager Erc color camera.
876
877 **Asdf Quantification.** ORO-stained worms were placed on glass slides and a
878 coverslip was placed over the sample. Worms were scored, as previously
879 described (Stuhr et al., 2022). Worms were scored and images were taken with
880 the Zeiss Axio Imager Erc color camera at 5x magnification. Fat levels of worms
881 were placed into three categories: non-Asdf, intermediate, and Asdf. Non-Asdf
882 worms display no loss of fat and are stained dark red throughout most of the body
883 (somatic and germ cells). Intermediate worms display significant fat loss from the
884 somatic tissues, with portions of the intestine being clear, but ORO-stained fat
885 deposits are still visible (somatic < germ cells). Asdf worms had most, if not all,
886 observable somatic fat deposits depleted (germ cells only).
887
888 **Quantification and statistical analysis.** Unless otherwise indicated, the
889 statistical differences between control and experimental groups were determined
890 by two-tailed students *t*-test (two groups), one-way ANOVA (more than two
891 groups), or two-way ANOVA (two independent experimental variables), with
892 corrected P values < 0.05 considered significant. Analyses conducting more than
893 two comparisons were always corrected for multiple hypothesis testing. The log
894 rank test was used to determine significance in lifespan analyses using online
895 OASIS2.
896

Acknowledgments

We thank Talia Hart, Dr. Gary Ruvkun, Dr. Eric Greer, and Dr. Keith Blackwell for discussions and constructive criticisms. This work was funded by NIH/NIA Grants R01AG058259 and R01AG69677 (to A.A.S.) and R01AG058610 (to S.P.C.), by the Weissman Family MGH Research Scholar Award (to A.A.S.), by a NSF GRFP Award 1000253984 (to L.C.), and by NIH/NIAID R01AI130289 (to R.P.W.), and by IRACDA NIH Grant K12GM106996 (to L.C.). Thanks to the University of Southern California and Buck Institute Nathan Shock Center (P30AG068345) for providing core services and support. Thanks to the NIH/NIDDK-funded NORC of Harvard (P30DK040561) and the NIH/NIDDK-funded Boston-Area DERC (P30DK057521) for core services. Some strains were provided by the CGC, funded by the NIH Office of Research Infrastructure Programs (P40OD010440), and the *C. elegans* Knockout Consortium. Figures 1A, 3C, and 7A were created with BioRender.com.

References

Albert, C.J., Thukkani, A.K., Heuertz, R.M., Slungaard, A., Hazen, S.L., and Ford, D.A. 2003. Eosinophil peroxidase-derived reactive brominating species target the vinyl ether bond of plasmalogens generating a novel chemoattractant, alpha-bromo fatty aldehyde. J Biol Chem *278*, 8942-8950. doi: 10.1074/jbc.m211634200, PubMed PMID: 12643282.

Albert, D.H., and Anderson, C.E. 1977. Ether-linked glycerolipids in human brain tumors. Lipids *12*, 188-192. doi: 10.1007/bf02533292, PubMed PMID: 846302.

Apfeld, J., O'Connor, G., McDonagh, T., DiStefano, P.S., and Curtis, R. 2004. The AMP-activated protein kinase AAK-2 links energy levels and insulin-like signals to lifespan in C. elegans. Genes Dev *18*, 3004-3009. PMC535911. doi: 10.1101/gad.1255404, PubMed PMID: 15574588.

Arthur, G., and Bittman, R. 2014. Glycosylated antitumor ether lipids: activity and mechanism of action. Anticancer Agents Med Chem *14*, 592-606. doi: 10.2174/1871520614666140309231144, PubMed PMID: 24628233.

Barzilai, N., Crandall, J.P., Kritchevsky, S.B., and Espeland, M.A. 2016. Metformin as a tool to target aging. Cell metabolism *23*, 1060-1065. doi, PubMed PMID.

Benjamin, D.I., Cozzo, A., Ji, X., Roberts, L.S., Louie, S.M., Mulvihill, M.M., Luo, K., and Nomura, D.K. 2013. Ether lipid generating enzyme AGPS alters the balance of structural and signaling lipids to fuel cancer pathogenicity. Proc Natl Acad Sci U S A *110*, 14912-14917. PMC3773741. doi: 10.1073/pnas.1310894110, PubMed PMID: 23980144.

Benjamini, Y., and Hochberg, Y. 1995. Controlling the False Discovery Rate: A Practical and Powerful Approach to Multiple Testing. Journal of the Royal Statistical Society Series B (Methodological) *57*, 289-300. doi, PubMed PMID.

Braverman, N., Steel, G., Obie, C., Moser, A., Moser, H., Gould, S.J., and Valle, D. 1997. Human PEX7 encodes the peroxisomal PTS2 receptor and is responsible for rhizomelic chondrodysplasia punctata. Nature genetics *15*, 369-376. doi, PubMed PMID.

Cabreiro, F., Au, C., Leung, K.-Y., Vergara-Irigaray, N., Cochemé, H.M., Noori, T., Weinkove, D., Schuster, E., Greene, N.D., and Gems, D. 2013. Metformin retards aging in C. elegans by altering microbial folate and methionine metabolism. Cell *153*, 228-239. doi, PubMed PMID.

944 Chen, J., Ou, Y., Li, Y., Hu, S., Shao, L.-W., and Liu, Y. 2017. Metformin extends C.
945 elegans lifespan through lysosomal pathway. Elife *6*, e31268. doi, PubMed PMID.
946 Curtis, R., O'Connor, G., and DiStefano, P.S. 2006. Aging networks in Caenorhabditis
947 elegans: AMP-activated protein kinase (aak-2) links multiple aging and metabolism
948 pathways. Aging Cell *5*, 119-126. doi: https://doi.org/10.1111/j.1474-9726.2006.00205.x,
949 PubMed PMID.
950 Davies, S.S., Pontsler, A.V., Marathe, G.K., Harrison, K.A., Murphy, R.C., Hinshaw, J.C.,
951 Prestwich, G.D., Hilaire, A.S., Prescott, S.M., and Zimmerman, G.A. 2001. Oxidized alkyl
952 phospholipids are specific, high affinity peroxisome proliferator-activated receptor γ
953 ligands and agonists. Journal of Biological Chemistry *276*, 16015-16023. doi, PubMed
954 PMID.
955 Dean, J.M., and Lodhi, I.J. 2018. Structural and functional roles of ether lipids. Protein
956 Cell *9*, 196-206. PMC5818364. doi: 10.1007/s13238-017-0423-5, PubMed PMID:
957 28523433.
958 Drechsler, R., Chen, S.W., Dancy, B.C., Mehrabkhani, L., and Olsen, C.P. 2016. HPLC-
959 Based Mass Spectrometry Characterizes the Phospholipid Alterations in Ether-Linked
960 Lipid Deficiency Models Following Oxidative Stress. PLoS One *11*, e0167229.
961 PMC5125691. doi: 10.1371/journal.pone.0167229, PubMed PMID: 27893806.
962 Evans, J.M., Donnelly, L.A., Emslie-Smith, A.M., Alessi, D.R., and Morris, A.D. 2005.
963 Metformin and reduced risk of cancer in diabetic patients. Bmj *330*, 1304-1305. doi,
964 PubMed PMID.
965 Facciotti, F., Ramanjaneyulu, G.S., Lepore, M., Sansano, S., Cavallari, M., Kistowska,
966 M., Forss-Petter, S., Ni, G., Colone, A., and Singhal, A. 2012. Peroxisome-derived lipids
967 are self antigens that stimulate invariant natural killer T cells in the thymus. Nature
968 immunology *13*, 474-480. doi, PubMed PMID.
969 Ghosh, M.K., and Hajra, A.K. 1986. Subcellular distribution and properties of acyl/alkyl
970 dihydroxyacetone phosphate reductase in rodent livers. Archives of biochemistry and
971 biophysics *245*, 523-530. doi, PubMed PMID.
972 Glaser, P.E., and Gross, R.W. 1994. Plasmenylethanolamine facilitates rapid membrane
973 fusion: a stopped-flow kinetic investigation correlating the propensity of a major plasma
974 membrane constituent to adopt an HII phase with its ability to promote membrane fusion.
975 Biochemistry *33*, 5805-5812. doi, PubMed PMID.
976 Gonzalez-Covarrubias, V., Beekman, M., Uh, H.W., Dane, A., Troost, J., Paliukhovich, I.,
977 van der Kloet, F.M., Houwing-Duistermaat, J., Vreeken, R.J., Hankemeier, T.*, et al.*
978 2013. Lipidomics of familial longevity. Aging Cell *12*, 426-434. PMC3709127. doi:
979 10.1111/acel.12064, PubMed PMID: 23451766.
980 Goodenowe, D.B., Cook, L.L., Liu, J., Lu, Y., Jayasinghe, D.A., Ahiahonu, P.W., Heath,
981 D., Yamazaki, Y., Flax, J., Krenitsky, K.F.*, et al.* 2007. Peripheral ethanolamine
982 plasmalogen deficiency: a logical causative factor in Alzheimer's disease and dementia.
983 J Lipid Res *48*, 2485-2498. doi: 10.1194/jlr.P700023-JLR200, PubMed PMID:
984 17664527.
985 Grimm, M.O., Grösgen, S., Riemenschneider, M., Tanila, H., Grimm, H.S., and
986 Hartmann, T. 2011. From brain to food: analysis of phosphatidylcholins, lyso-
987 phosphatidylcholins and phosphatidylcholin-plasmalogens derivates in Alzheimer's
988 disease human post mortem brains and mice model via mass spectrometry. J
989 Chromatogr A *1218*, 7713-7722. doi: 10.1016/j.chroma.2011.07.073, PubMed PMID:
990 21872257.
991 Han, S.K., Lee, D., Lee, H., Kim, D., Son, H.G., Yang, J.S., Lee, S.V., and Kim, S. 2016.
992 OASIS 2: online application for survival analysis 2 with features for the analysis of

993 maximal lifespan and healthspan in aging research. Oncotarget *7*, 56147-56152.
994 5302902. doi: 10.18632/oncotarget.11269, PubMed PMID: 27528229.
995 Han, X., Holtzman, D.M., and McKeel, D.W., Jr. 2001. Plasmalogen deficiency in early
996 Alzheimer's disease subjects and in animal models: molecular characterization using
997 electrospray ionization mass spectrometry. J Neurochem *77*, 1168-1180. doi:
998 10.1046/j.1471-4159.2001.00332.x, PubMed PMID: 11359882.
999 Hardeman, D., and Van den Bosch, H. 1989. Topography of ether phospholipid
1000 biosynthesis. Biochimica et Biophysica Acta (BBA)-Lipids and Lipid Metabolism *1006*, 1-
1001 8. doi, PubMed PMID.
1002 Hermann, G.J., Schroeder, L.K., Hieb, C.A., Kershner, A.M., Rabbitts, B.M., Fonarev, P.,
1003 Grant, B.D., and Priess, J.R. 2005. Genetic analysis of lysosomal trafficking in
1004 Caenorhabditis elegans. Mol Biol Cell *16*, 3273-3288. PMC1165410. doi:
1005 10.1091/mbc.e05-01-0060, PubMed PMID: 15843430.
1006 Honsho, M., Asaoku, S., and Fujiki, Y. 2010. Posttranslational regulation of fatty acyl-
1007 CoA reductase 1, Far1, controls ether glycerophospholipid synthesis. J Biol Chem *285*,
1008 8537-8542. PMC2838275. doi: 10.1074/jbc.M109.083311, PubMed PMID: 20071337.
1009 Horikawa, M., Nomura, T., Hashimoto, T., and Sakamoto, K. 2008. Elongation and
1010 desaturation of fatty acids are critical in growth, lipid metabolism and ontogeny of
1011 Caenorhabditis elegans. J Biochem *144*, 149-158. doi: 10.1093/jb/mvn055, PubMed
1012 PMID: 18424809.
1013 Hua, R., Cheng, D., Coyaud, É., Freeman, S., Di Pietro, E., Wang, Y., Vissa, A., Yip,
1014 C.M., Fairn, G.D., and Braverman, N. 2017. VAPs and ACBD5 tether peroxisomes to the
1015 ER for peroxisome maintenance and lipid homeostasis. Journal of Cell Biology *216*, 367-
1016 377. doi, PubMed PMID.
1017 Inzucchi, S.E., Bergenstal, R.M., Buse, J.B., Diamant, M., Ferrannini, E., Nauck, M.,
1018 Peters, A.L., Tsapas, A., Wender, R., and Matthews, D.R. 2012. Management of
1019 hyperglycaemia in type 2 diabetes: a patient-centered approach. Position statement of
1020 the American Diabetes Association (ADA) and the European Association for the Study of
1021 Diabetes (EASD). Diabetologia *55*, 1577-1596. doi, PubMed PMID.
1022 Itzkovitz, B., Jiralerspong, S., Nimmo, G., Loscalzo, M., Horovitz, D.D., Snowden, A.,
1023 Moser, A., Steinberg, S., and Braverman, N. 2012. Functional characterization of novel
1024 mutations in GNPAT and AGPS, causing rhizomelic chondrodysplasia punctata (RCDP)
1025 types 2 and 3. Hum Mutat *33*, 189-197. doi: 10.1002/humu.21623, PubMed PMID:
1026 21990100.
1027 Jaffrès, P.A., Gajate, C., Bouchet, A.M., Couthon-Gourvès, H., Chantôme, A., Potier-
1028 Cartereau, M., Besson, P., Bougnoux, P., Mollinedo, F., and Vandier, C. 2016. Alkyl
1029 ether lipids, ion channels and lipid raft reorganization in cancer therapy. Pharmacol Ther
1030 *165*, 114-131. doi: 10.1016/j.pharmthera.2016.06.003, PubMed PMID: 27288726.
1031 Kamath, R.S., and Ahringer, J. 2003. Genome-wide RNAi screening in Caenorhabditis
1032 elegans. Methods *30*, 313-321. doi, PubMed PMID: 12828945.
1033 Kenyon, C., Chang, J., Gensch, E., Rudner, A., and Tabtiang, R. 1993. A C. elegans
1034 mutant that lives twice as long as wild type. Nature *366*, 461-464. doi:
1035 10.1038/366461a0, PubMed PMID: 8247153.
1036 Komljenovic, D., Sandhoff, R., Teigler, A., Heid, H., Just, W.W., and Gorgas, K. 2009.
1037 Disruption of blood-testis barrier dynamics in ether-lipid-deficient mice. Cell and tissue
1038 research *337*, 281-299. doi, PubMed PMID.
1039 Lynn, D.A., Dalton, H.M., Sowa, J.N., Wang, M.C., Soukas, A.A., and Curran, S.P. 2015.
1040 Omega-3 and -6 fatty acids allocate somatic and germline lipids to ensure fitness during
1041 nutrient and oxidative stress in Caenorhabditis elegans. Proc Natl Acad Sci U S A *112*,

1042 15378-15383. PMC4687584. doi: 10.1073/pnas.1514012112, PubMed PMID:
1043 26621724.
1044 Maeba, R., Sawada, Y., Shimasaki, H., Takahashi, I., and Ueta, N. 2002. Ethanolamine
1045 plasmalogens protect cholesterol-rich liposomal membranes from oxidation caused by
1046 free radicals. Chem Phys Lipids *120*, 145-151. doi: 10.1016/s0009-3084(02)00101-9,
1047 PubMed PMID: 12426083.
1048 Marrink, S.-J., and Mark, A.E. 2004. Molecular view of hexagonal phase formation in
1049 phospholipid membranes. Biophysical journal *87*, 3894-3900. doi, PubMed PMID.
1050 Martin-Montalvo, A., Mercken, E.M., Mitchell, S.J., Palacios, H.H., Mote, P.L., Scheibye-
1051 Knudsen, M., Gomes, A.P., Ward, T.M., Minor, R.K., and Blouin, M.-J. 2013. Metformin
1052 improves healthspan and lifespan in mice. Nature communications *4*, 1-9. doi, PubMed
1053 PMID.
1054 Mitchell, T.W., Buffenstein, R., and Hulbert, A.J. 2007. Membrane phospholipid
1055 composition may contribute to exceptional longevity of the naked mole-rat
1056 (Heterocephalus glaber): a comparative study using shotgun lipidomics. Exp Gerontol
1057 *42*, 1053-1062. doi: 10.1016/j.exger.2007.09.004, PubMed PMID: 18029129.
1058 Morand, O.H., Zoeller, R.A., and Raetz, C.R. 1988. Disappearance of plasmalogens
1059 from membranes of animal cells subjected to photosensitized oxidation. J Biol Chem
1060 *263*, 11597-11606. doi, PubMed PMID: 3403548.
1061 Motley, A.M., Hettema, E.H., Hogenhout, E.M., Brites, P., ten Asbroek, A.L., Wijburg,
1062 F.A., Baas, F., Heijmans, H.S., Tabak, H.F., and Wanders, R.J. 1997. Rhizomelic
1063 chondrodysplasia punctata is a peroxisomal protein targeting disease caused by a non-
1064 functional PTS2 receptor. Nature genetics *15*, 377-380. doi, PubMed PMID.
1065 Munro, D., and Blier, P.U. 2012. The extreme longevity of Arctica islandica is associated
1066 with increased peroxidation resistance in mitochondrial membranes. Aging Cell *11*, 845-
1067 855. doi: 10.1111/j.1474-9726.2012.00847.x, PubMed PMID: 22708840.
1068 Nhan, J.D., Turner, C.D., Anderson, S.M., Yen, C.A., Dalton, H.M., Cheesman, H.K.,
1069 Ruter, D.L., Uma Naresh, N., Haynes, C.M., Soukas, A.A*., et al.* 2019. Redirection of
1070 SKN-1 abates the negative metabolic outcomes of a perceived pathogen infection. Proc
1071 Natl Acad Sci U S A *116*, 22322-22330. PMC6825279. doi: 10.1073/pnas.1909666116,
1072 PubMed PMID: 31611372.
1073 Onken, B., and Driscoll, M. 2010. Metformin induces a dietary restriction–like state and
1074 the oxidative stress response to extend C. elegans healthspan via AMPK, LKB1, and
1075 SKN-1. PloS one *5*, e8758. doi, PubMed PMID.
1076 Pang, Z., Chong, J., Zhou, G., de Lima Morais, D.A., Chang, L., Barrette, M., Gauthier,
1077 C., Jacques, P.-É., Li, S., and Xia, J. 2021. MetaboAnalyst 5.0: narrowing the gap
1078 between raw spectra and functional insights. Nucleic Acids Research *49*, W388-W396.
1079 doi: 10.1093/nar/gkab382, PubMed PMID.
1080 Perez, C.L., and Van Gilst, M.R. 2008. A 13C isotope labeling strategy reveals the
1081 influence of insulin signaling on lipogenesis in C. elegans. Cell Metab *8*, 266-274. doi:
1082 10.1016/j.cmet.2008.08.007, PubMed PMID: 18762027.
1083 Perez, M.A., Magtanong, L., Dixon, S.J., and Watts, J.L. 2020. Dietary Lipids Induce
1084 Ferroptosis in Caenorhabditiselegans and Human Cancer Cells. Dev Cell *54*, 447-
1085 454.e444. PMC7483868. doi: 10.1016/j.devcel.2020.06.019, PubMed PMID: 32652074.
1086 Perez, M.A., and Watts, J.L. 2021. Worms, Fat, and Death: Caenorhabditis elegans
1087 Lipid Metabolites Regulate Cell Death. Metabolites *11*. PMC7926963. doi:
1088 10.3390/metabo11020125, PubMed PMID: 33672292.

1089 Petrascheck, M., and Miller, D.L. 2017. Computational Analysis of Lifespan Experiment
1090 Reproducibility. Front Genet *8*, 92. PMC5492194. doi: 10.3389/fgene.2017.00092,
1091 PubMed PMID: 28713422.
1092 Pino, E.C., and Soukas, A.A. 2020. Quantitative Profiling of Lipid Species in
1093 Caenorhabditis elegans with Gas Chromatography-Mass Spectrometry. Methods Mol
1094 Biol *2144*, 111-123. doi: 10.1007/978-1-0716-0592-9_10, PubMed PMID: 32410029.
1095 Pino, E.C., Webster, C.M., Carr, C.E., and Soukas, A.A. 2013. Biochemical and high
1096 throughput microscopic assessment of fat mass in Caenorhabditis elegans. J Vis Exp.
1097 PMC3944676. doi: 10.3791/50180, PubMed PMID: 23568026.
1098 Pradas, I., Jové, M., Huynh, K., Puig, J., Inglés, M., Borrás, C., Viña, J., Meikle, P.J., and
1099 Pamplona, R. 2019. Exceptional human longevity is associated with a specific plasma
1100 phenotype of ether lipids. Redox biology *21*, 101127. doi, PubMed PMID.
1101 Purdue, P.E., Zhang, J.W., Skoneczny, M., and Lazarow, P.B. 1997. Rhizomelic
1102 chondrodysplasia punctata is caused by deficiency of human PEX7, a homologue of the
1103 yeast PTS2 receptor. Nature genetics *15*, 381-384. doi, PubMed PMID.
1104 Reiss, D., Beyer, K., and Engelmann, B. 1997. Delayed oxidative degradation of
1105 polyunsaturated diacyl phospholipids in the presence of plasmalogen phospholipids in
1106 vitro. Biochem J *323 (Pt 3)*, 807-814. PMC1218386. doi: 10.1042/bj3230807, PubMed
1107 PMID: 9169616.
1108 Rodemer, C., Thai, T.P., Brugger, B., Kaercher, T., Werner, H., Nave, K.A., Wieland, F.,
1109 Gorgas, K., and Just, W.W. 2003. Inactivation of ether lipid biosynthesis causes male
1110 infertility, defects in eye development and optic nerve hypoplasia in mice. Hum Mol
1111 Genet *12*, 1881-1895. doi: 10.1093/hmg/ddg191, PubMed PMID: 12874108.
1112 Sakamoto, T., Maebayashi, K., Nakagawa, Y., and Imai, H. 2014. Deletion of the four
1113 phospholipid hydroperoxide glutathione peroxidase genes accelerates aging in
1114 Caenorhabditis elegans. Genes Cells *19*, 778-792. doi: 10.1111/gtc.12175, PubMed
1115 PMID: 25200408.
1116 Schreiber, M.A., Pierce-Shimomura, J.T., Chan, S., Parry, D., and McIntire, S.L. 2010.
1117 Manipulation of behavioral decline in Caenorhabditis elegans with the Rag GTPase
1118 raga-1. PLoS Genet *6*, e1000972. PMC2877737. doi: 10.1371/journal.pgen.1000972,
1119 PubMed PMID: 20523893.
1120 Segal, E.D., Yasmeen, A., Beauchamp, M.C., Rosenblatt, J., Pollak, M., and Gotlieb,
1121 W.H. 2011. Relevance of the OCT1 transporter to the antineoplastic effect of biguanides.
1122 Biochem Biophys Res Commun *414*, 694-699. doi: 10.1016/j.bbrc.2011.09.134,
1123 PubMed PMID: 21986525.
1124 Senchuk, M.M., Dues, D.J., Schaar, C.E., Johnson, B.K., Madaj, Z.B., Bowman, M.J.,
1125 Winn, M.E., and Van Raamsdonk, J.M. 2018. Activation of DAF-16/FOXO by reactive
1126 oxygen species contributes to longevity in long-lived mitochondrial mutants in
1127 Caenorhabditis elegans. PLoS Genet *14*, e1007268. PMC5862515. doi:
1128 10.1371/journal.pgen.1007268, PubMed PMID: 29522556.
1129 Shi, X., Tarazona, P., Brock, T.J., Browse, J., Feussner, I., and Watts, J.L. 2016. A
1130 Caenorhabditis elegans model for ether lipid biosynthesis and function. Journal of lipid
1131 research *57*, 265-275. doi, PubMed PMID.
1132 Shmookler Reis, R.J., Xu, L., Lee, H., Chae, M., Thaden, J.J., Bharill, P., Tazearslan, C.,
1133 Siegel, E., Alla, R., Zimniak, P.*, et al.* 2011. Modulation of lipid biosynthesis contributes
1134 to stress resistance and longevity of C. elegans mutants. Aging (Albany NY) *3*, 125-147.
1135 PMC3082008. doi: 10.18632/aging.100275, PubMed PMID: 21386131.

1136 Singh, H., Beckman, K., and Poulos, A. 1993. Exclusive localization in peroxisomes of
1137 dihydroxyacetone phosphate acyltransferase and alkyl-dihydroxyacetone phosphate
1138 synthase in rat liver. Journal of lipid research *34*, 467-477. doi, PubMed PMID.
1139 Snyder, F., and Wood, R. 1969. Alkyl and alk-1-enyl ethers of glycerol in lipids from
1140 normal and neoplastic human tissues. Cancer Res *29*, 251-257. doi, PubMed PMID:
1141 5763979.
1142 Sogame, Y., Kitamura, A., Yabuki, M., and Komuro, S. 2009. A comparison of uptake of
1143 metformin and phenformin mediated by hOCT1 in human hepatocytes. Biopharm Drug
1144 Dispos *30*, 476-484. doi: 10.1002/bdd.684, PubMed PMID: 19768675.
1145 Soukas, A.A., Kane, E.A., Carr, C.E., Melo, J.A., and Ruvkun, G. 2009. Rictor/TORC2
1146 regulates fat metabolism, feeding, growth, and life span in Caenorhabditis elegans.
1147 Genes & development *23*, 496-511. doi, PubMed PMID.
1148 Stirling, D.R., Swain-Bowden, M.J., Lucas, A.M., Carpenter, A.E., Cimini, B.A., and
1149 Goodman, A. 2021. CellProfiler 4: improvements in speed, utility and usability. BMC
1150 Bioinformatics *22*, 433. PMC8431850. doi: 10.1186/s12859-021-04344-9, PubMed
1151 PMID: 34507520.
1152 Stuhr, N.L., Nhan, J.D., Hammerquist, A.M., Van Camp, B., Reoyo, D., and Curran, S.P.
1153 2022. Rapid Lipid Quantification in Caenorhabditis elegans by Oil Red O and Nile Red
1154 Staining. Bio Protoc *12*, e4340. PMC8918222. doi: 10.21769/BioProtoc.4340, PubMed
1155 PMID: 35592599.
1156 Teigler, A., Komljenovic, D., Draguhn, A., Gorgas, K., and Just, W.W. 2009. Defects in
1157 myelination, paranode organization and Purkinje cell innervation in the ether lipid-
1158 deficient mouse cerebellum. Hum Mol Genet *18*, 1897-1908. PMC2722228. doi:
1159 10.1093/hmg/ddp110, PubMed PMID: 19270340.
1160 Thukkani, A.K., Hsu, F.F., Crowley, J.R., Wysolmerski, R.B., Albert, C.J., and Ford, D.A.
1161 2002. Reactive chlorinating species produced during neutrophil activation target tissue
1162 plasmalogens: production of the chemoattractant, 2-chlorohexadecanal. J Biol Chem
1163 *277*, 3842-3849. doi: 10.1074/jbc.M109489200, PubMed PMID: 11724792.
1164 Watts, J.L. 2016. Using Caenorhabditis elegans to Uncover Conserved Functions of
1165 Omega-3 and Omega-6 Fatty Acids. Journal of Clinical Medicine *5*, 19. doi, PubMed
1166 PMID: doi:10.3390/jcm5020019.
1167 White, A.L., Modaff, P., Holland-Morris, F., and Pauli, R.M. 2003. Natural history of
1168 rhizomelic chondrodysplasia punctata. Am J Med Genet A *118a*, 332-342. doi:
1169 10.1002/ajmg.a.20009, PubMed PMID: 12687664.
1170 Wu, L., Zhou, B., Oshiro-Rapley, N., Li, M., Paulo, J.A., Webster, C.M., Mou, F.,
1171 Kacergis, M.C., Talkowski, M.E., and Carr, C.E. 2016. An ancient, unified mechanism for
1172 metformin growth inhibition in C. elegans and cancer. Cell *167*, 1705-1718. e1713. doi,
1173 PubMed PMID.
1174 Yuan, P., Ito, K., Perez-Lorenzo, R., Del Guzzo, C., Lee, J.H., Shen, C.-H., Bosenberg,
1175 M.W., McMahon, M., Cantley, L.C., and Zheng, B. 2013. Phenformin enhances the
1176 therapeutic benefit of BRAFV600E inhibition in melanoma. Proceedings of the National
1177 Academy of Sciences *110*, 18226-18231. doi, PubMed PMID.
1178 Zhang, S.O., Box, A.C., Xu, N., Le Men, J., Yu, J., Guo, F., Trimble, R., and Mak, H.Y.
1179 2010a. Genetic and dietary regulation of lipid droplet expansion in Caenorhabditis
1180 elegans. Proc Natl Acad Sci U S A *107*, 4640-4645. PMC2842062. doi:
1181 10.1073/pnas.0912308107, PubMed PMID: 20176933.
1182 Zhang, S.O., Trimble, R., Guo, F., and Mak, H.Y. 2010b. Lipid droplets as ubiquitous fat
1183 storage organelles in C. elegans. BMC Cell Biol *11*, 96. PMC3004847. doi:
1184 10.1186/1471-2121-11-96, PubMed PMID: 21143850.

1185 Zoeller, R.A., Morand, O.H., and Raetz, C.R. 1988. A possible role for plasmalogens in
1186 protecting animal cells against photosensitized killing. J Biol Chem *263*, 11590-11596.
1187 doi, PubMed PMID: 3403547.
1188 Zou, Y., Henry, W.S., Ricq, E.L., Graham, E.T., Phadnis, V.V., Maretich, P., Paradkar,
1189 S., Boehnke, N., Deik, A.A., Reinhardt, F.*, et al.* 2020. Plasticity of ether lipids promotes
1190 ferroptosis susceptibility and evasion. Nature *585*, 603-608. PMC8051864. doi:
1191 10.1038/s41586-020-2732-8, PubMed PMID: 32939090.

1192 **Supplementary material for this manuscript includes 5 figures and 2**
1193 **supplementary files.**
1194
1195 **Supplementary file descriptions:**
1196
1197 **Supplementary file 1 (separate file).** Tabular and survival data including 3
1198 biological replicates (unless otherwise noted) are shown for lifespan experiments
1199 related to Figures 1, 3, 4, 5, Figure 1- figure supplement 1, Figure 4- figure
1200 supplement 1, and Figure 5- figure supplement 1. Data present a summary of the
1201 conditions tested which, if applicable, include: (1) drug treatment with vehicle
1202 control and 4.5 mM phenformin or 50 mM metformin and/or (2) RNAi treatment to
1203 knockdown expression of the specific denoted gene. The *C. elegans* strain,
1204 number of subjects, restricted mean (days), standard error, 95% confidence
1205 interval (C.I.), 95% median C.I., and *P*-values for relevant comparisons are noted
1206 amongst all conditions. ns, not significant; *, $P < 0.05$; **, $P < 0.01$; ***, $P < 0.001$;
1207 ****, $P < 0.0001$ by log-rank analysis.
1208
1209 **Supplementary file 2 (separate file).** Excel file containing raw, normalized, and
1210 normalized and $\log_{10}$ transformed mass spectrometry data for
1211 phosphatidylethanolamine containing ether lipids detected by LC-MS/MS. Data
1212 from **3** biological replicates are shown for molecules indicated for vehicle or 4.5
1213 mM phenformin treatment, for 4 different genetic backgrounds: wild type animals
1214 (N2), BX10 (*ads-1* mutant), BX259 (*acl-7* mutant) and BX275 (*fard-1* mutant).
1215 Compound identity for each detected lipid as well as raw, normalized or
1216 transformed mass counts on each of three tabs. Note**,** several of the lipids were
1217 not uniformly detected or of low abundance, and thus were filtered by the
1218 MetaboAnalyst parameters used and not represented on the “Normalized” and
1219 “Normalized-Log10 Transformed” tabs.
1220

1221 **Figure 1—figure supplement 1**

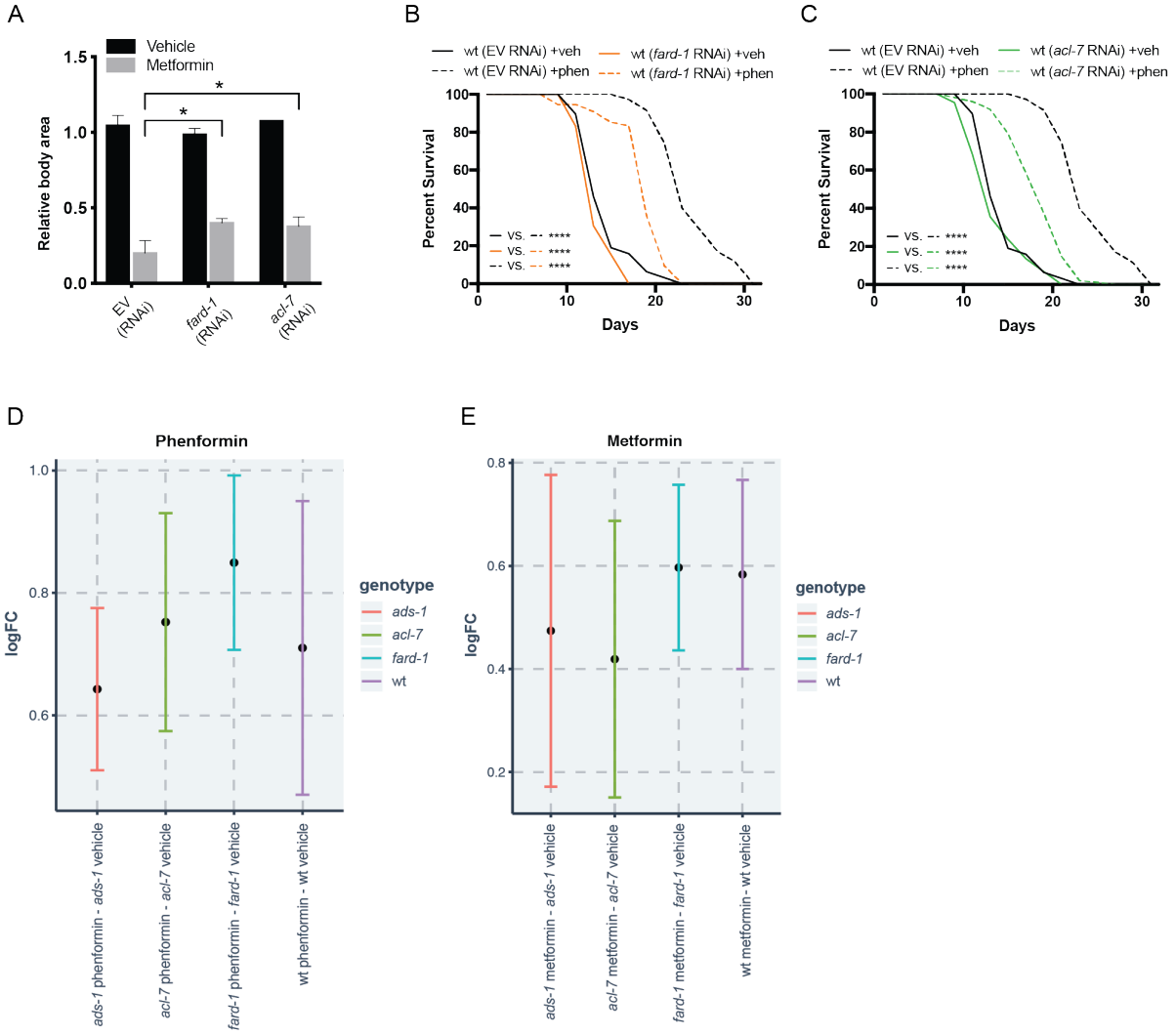

1222 **Figure 1—figure supplement 1. Reduced function of genes responsible for ether**
1223 **lipid biosynthesis partially suppresses biguanide effects of growth and lifespan**
1224 **without affecting biguanide levels.** (A) RNAi to *fard-1* and *acl-7* induce *C. elegans*
1225 resistance to growth inhibition by 160 mM metformin treatment. *, $P < 0.05$, by two-way
1226 ANOVA, n = 2 biological replicates. (B-C) RNAi knockdown of *fard-1* (*B*) and *acl-7* (*C*) in
1227 *C. elegans* partially suppresses phenformin's effect on lifespan extension. For *B* and *C,*
1228 results are representative of 3 biological replicates. ****, $P < 0.0001$ by log-rank analysis;
1229 for tabular survival data and biological replicates see also Supplementary file 1. (D) Log
1230 fold change (LogFC) of phenformin abundance in samples treated with 4.5 mM
1231 phenformin versus vehicle reveals that the increase in phenformin levels in wild type and
1232 three ether lipid deficient mutants is similar. (E) LogFC of metformin abundance in
1233 samples treated with 50 mM metformin versus vehicle show that metformin increases are
1234 similar across all 4 strains (*E*). Bars represent mean and 95% confidence intervals.

1235 **Figure 2—figure supplement 1**

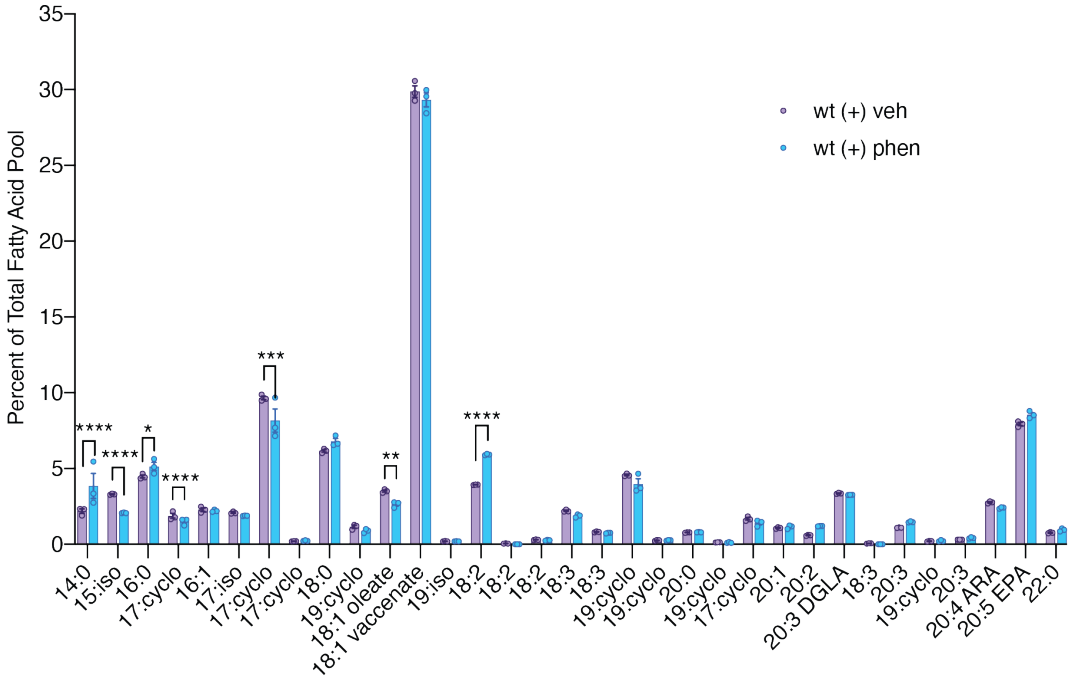

1236 **Figure 2—figure supplement 1. Biguanide treatment modulates abundance of fatty**
1237 **acids in *C. elegans.*** A comparison of the percent of the total fatty acid pool for 33 fatty
1238 acids shows that 7 fatty acids are significantly altered in phenformin treated wild type
1239 worms. n = 3 biological replicates. *, $P < 0.05$; **, $P < 0.01$; ***, $P < 0.001$; ****, $P < 0.0001$
1240 by multiple t-tests (corrected for multiple hypothesis testing with two-stage step-up method
1241 of Benjamini, Krieger, and Yekutieli).

1242 **Figure 2—figure supplement 2**

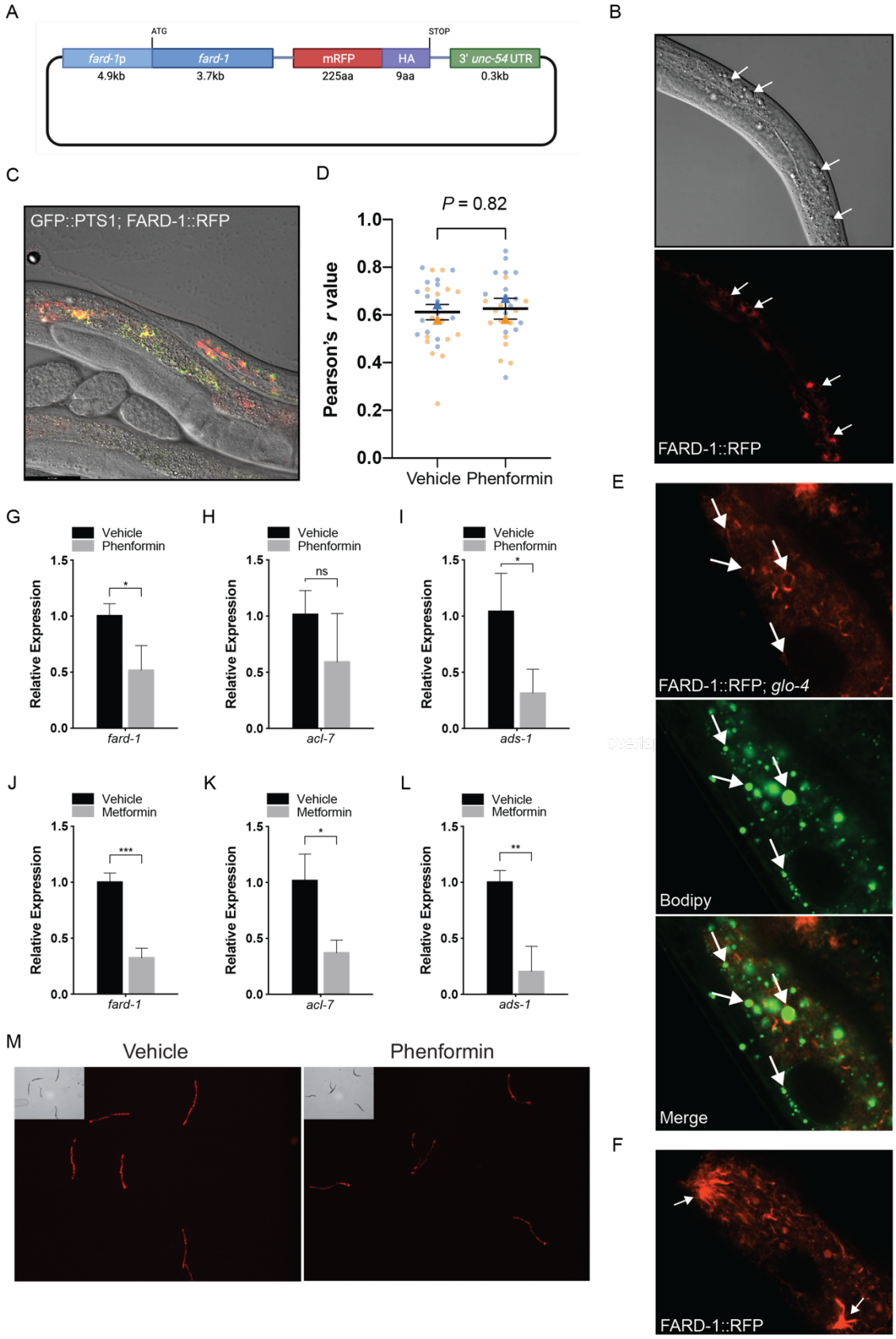

1243 **Figure 2—figure supplement 2. FARD-1::RFP localizes to intestinal lipid droplets**
1244 **and peroxisomes and is not positively regulated at the RNA or protein level by**
1245 **phenformin.** (A) Diagram of the *C. elegans* FARD-1::RFP overexpression reporter. (B)
1246 FARD-1::RFP *(fard-1 oe1)* exhibits intestinal expression in *C. elegans*. FARD-1 displays
1247 a cytoplasmic distribution and an association with structures resembling lipid droplets (B*,*
1248 *arrows*). (C) Co-expression of FARD-1::RFP and peroxisomally targeted GFP::PTS1 in
1249 transgenic animals indicates partial colocalization of FARD-1 with peroxisomes in
1250 intestine. (D) Superplot displays colocalization of RFP and GFP in vehicle or phenformin
1251 treated GFP::PTS1; FARD-1::RFP transgenics (N= 20 total worms assessed; 5 worms per
1252 condition; 3 images per worm (upper/mid/lower intestine)) for a total of 15 images (dots)
1253 per replicate; blue = replicate 1, orange = replicate 2). Correlation coefficients were
1254 separately calculated for each biological replicate and the mean is represented for each
1255 pool (blue or orange triangle). These two means were then used to calculate the average
1256 (horizontal bar), standard error of the mean (error bars), and P value. Analysis of the
1257 average Pearson's r values demonstrates no significant difference between colocalization
1258 of FARD-1::RFP and GFP::PTS1 in vehicle or phenformin-treated worms. n = 2 biological
1259 replicates. (E) Confocal imaging of an integrated FARD-1::RFP reporter *(fard-1 oe3)* in *C.*
1260 *elegans* stained with C1-BODIPY-C12 (treated with *glo-4* RNAi to remove BODIPY
1261 positive lysosome related organelles) demonstrates localization of FARD-1 protein to the
1262 surface of lipid droplets in the worm intestine. (F) In *fard-1(oe3)* transgenics, confocal
1263 imaging indicates FARD-1::RFP organization into web-like structures and bright punctae
1264 that represent the intersection of these "webs". These structures may represent smooth
1265 endoplasmic reticulum. (G-I) Levels of *fard-1*, *acl-7*, and *ads-1* mRNA decrease in wild
1266 type *C. elegans* treated with 4.5 mM phenformin versus vehicle. n = 3 biological replicates;
1267 ns, not significant; *, $P < 0.05$ by unpaired *t*-test. (J-L) Levels of *fard-1*, *acl-7,* and *ads-1*
1268 mRNA decrease in wild type *C. elegans* treated with 50 mM metformin versus vehicle. n
1269 = 3 biological replicates; *, $P < 0.05$; **, $P < 0.01$; ***, $P < 0.001$ by unpaired *t*-test. (M)
1270 Phenformin (4.5 mM) results in decreased expression of the FARD-1::RFP translational
1271 reporter (*fard-1 oe1*). n = 3 biological replicates; total assessed: N = 30 worms per
1272 condition (10 worms per replicate).

1273 **Figure 4—figure supplement 1**

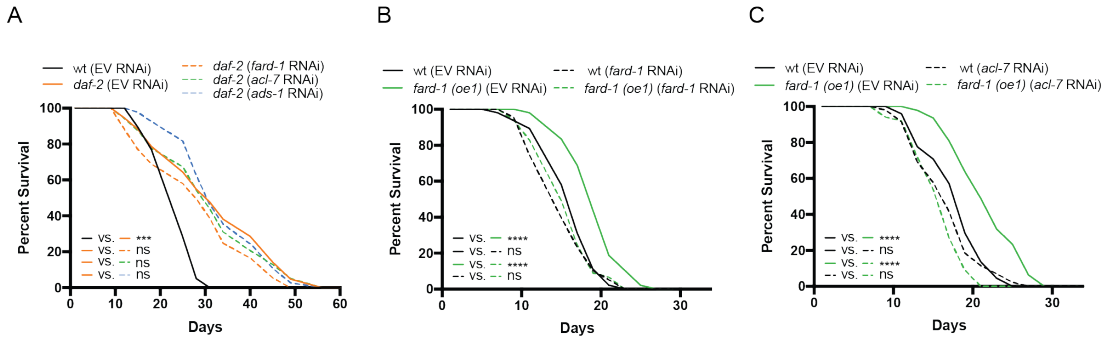

1274 **Figure 4—figure supplement 1. Ether lipid biosynthetic genes are not necessary for**
1275 ***daf-2*-dependent lifespan extension, and *fard-1* overexpression extends lifespan in**
1276 **a manner dependent upon ether lipid biosynthesis.** (A) *daf-2* mutants display extended
1277 lifespan relative to wild type animals. RNAi knockdown of *fard-1*, *acl-7*, and *ads-1* does
1278 not impact lifespan extension in these mutants. (B-C) RNAi knockdown of *fard-1* (*B*) and
1279 *acl-7* (*C*) suppresses *fard-1* overexpression*(oe1)*-associated lifespan extension. For A-C,
1280 results are representative of 2-3 biological replicates. ns, not significant; ***, $P < 0.001$;
1281 ****; $P < 0.0001$ by log-rank analysis. For tabular survival data and biological replicates
1282 see also Supplementary file 1.

1283 **Figure 5—figure supplement 1**

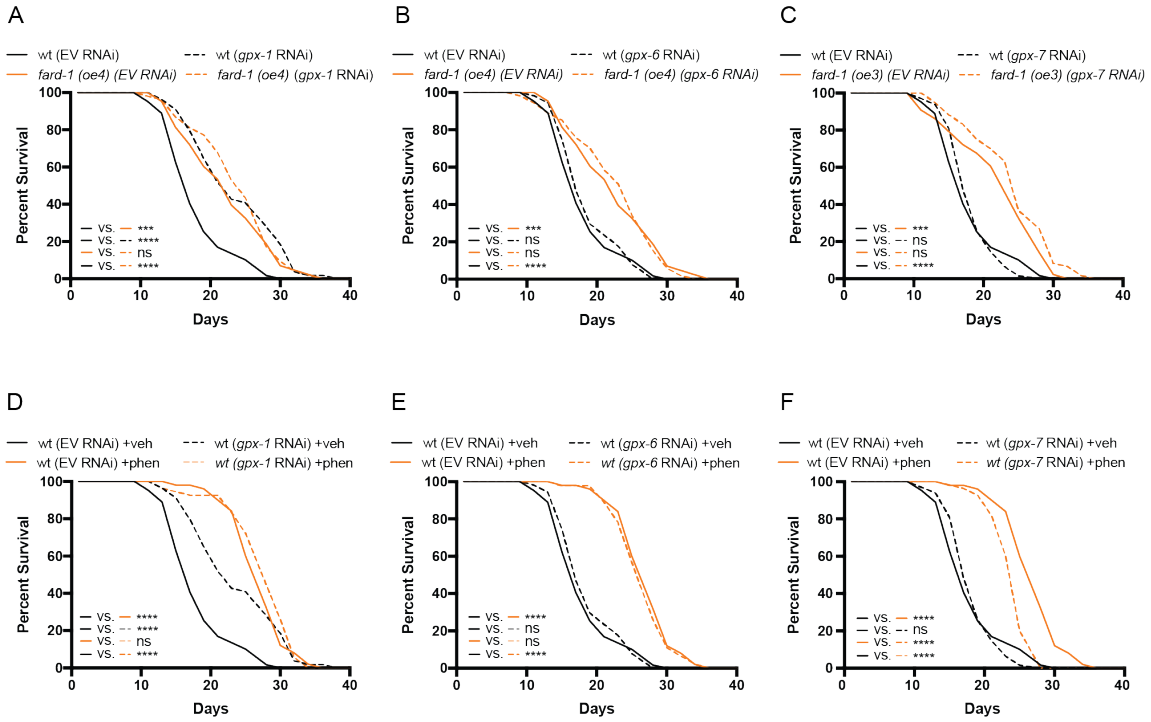

1284 **Figure 5—figure supplement 1. Genetic induction of ferroptosis does not impact**
1285 ***fard-1* overexpression nor biguanide-mediated lifespan extension.** (A-C)
1286 Independent knockdown of glutathione peroxidases, *gpx-1* (A), *gpx-6* (B), or *gpx-7* (C) by
1287 RNAi does not mitigate lifespan extension by integrated *fard-1* overexpression *(fard-1 oe3*
1288 and *fard-1 oe4)*, as would be expected if fard-1 overexpression extended lifespan by
1289 lowering ferroptosis. *gpx-1* unexpectedly extends lifespan in a non-additive manner with
1290 *fard-1(oe)*. (D-F) Similarly, knockdown of *gpx-1* (D), *gpx-6* (E), or *gpx-7* (F) by RNAi do
1291 not suppress phenformin-mediated lifespan extension. For *A-F,* results are representative
1292 of 2-3 biological replicates. ***, $P < 0.001$; ****, $P < 0.0001$ by log-rank analysis. For
1293 tabular survival data and biological replicates see also Supplementary file 1.